RESEARCH ARTICLE

Title: Epitranscriptome changes triggered by ammonium nutrition regulate the proteome response of maritime pine roots.

Authors: Francisco Ortigosa[#1], César Lobato-Fernández[#1], Juan Antonio Pérez-Claros[2], Francisco R. Cantón[1], Concepción Ávila[1], Francisco M. Cánovas[1], Rafael A. Cañas*[1].

Affiliations: [1]Grupo de Biología Molecular y Biotecnología de Plantas, Departamento de Biología Molecular y Bioquímica, Universidad de Málaga, Campus Universitario de Teatinos, 29071-Málaga, Spain

[2]Departamento de Ecología y Geología, Universidad de Málaga, Campus Universitario de Teatinos, 29071-Málaga, Spain

[#] These authors contributed equally to this work.

*Address correspondence to Rafael A. Cañas: rcanas@uma.es

Contact: Rafael A. Cañas**, email:** rcanas@uma.es, **Twitter:** @rcanas_a

Running title: Ammonium nutrition epitranscriptomics

ORCID: FO (0000-0002-7517-7594); CLF (0000-0001-9576-7236); JPC (0000-0002-9803-0085); FRC (0000-0001-6917-8630); CA (0000-0001-8817-7529); FMC (0000-0002-4914-2558) and RAC (0000-0001-9727-5585)

Total word count: 6981

ABSTRACT word count: 197

Proteomic data are available in PRIDE database for reviewer's login with:

Username: reviewer_pxd025331@ebi.ac.uk

Password: ASGRIYS5

ABSTRACT

Epitranscriptomic modifications constitute a gene expression checkpoint in all living organisms. As nitrogen is an essential element for plant growth and development, a reasonable hypothesis is that changes in the epitranscriptome may regulate nitrogen acquisition and metabolism. In this study, epitranscriptomic modifications caused by ammonium nutrition were monitored in maritime pine roots through direct RNA sequencing using Oxford Nanopore Technology. Transcriptomic responses mainly affected transcripts involved in nitrogen and carbon metabolism, defense, hormone synthesis/signaling, and translation. Global detection of epitranscriptomic marks was performed to evaluate this posttranscriptional mechanism in untreated and ammonium-treated seedlings. Increased m^6A deposition in the 3'-UTR was observed in response to ammonium, which seems to be correlated with poly(A) lengths and changes in the relative abundance of the corresponding proteins. The results showed that m^6A deposition and its dynamics seem to be important regulators of translation under ammonium nutrition. These findings suggest that protein translation is finely regulated through epitranscriptomic marks likely by changes in mRNA poly(A) length, transcript abundance and ribosome protein composition. An integration of multiomics data suggests that the epitranscriptome modulates responses to developmental and environmental changes, including ammonium nutrition, through buffering, filtering, and focusing the final products of gene expression.

Keywords: Nitrogen, ammonium, epitranscriptomics, ONT sequencing, maritime pine,

INTRODUCTION

Discoveries in the nascent field of molecular biology culminated in the central dogma of molecular biology during the 1970s (Crick, 1970). Currently, it is known that transcription and translation processes are not always directly linked. Multiple factors intervene in the gene response and its regulation. Two good examples of this are long noncoding RNAs (lncRNAs) (Liu et al., 2015) and microRNAs (miRNAs) (Paul et al., 2015). These types of RNA regulate important aspects of both development and response to external stimuli in plants (Liu et al., 2015; Paul et al., 2015). However, these studies represent only some aspects of overall RNA metabolism. In recent years, an increasing interest has focused on determining the biological role of RNA chemical modifications emerging as a new field of study under the term *epitranscriptomics*. These modifications are found in all RNA types, such as transfer RNAs (tRNAs), ribosomal RNAs (rRNAs), messenger RNAs (mRNAs) and small RNAs (RNAs) (Xiong et al., 2017). To date, more than 160 different modifications have been identified in RNA (Shen et al., 2019). In *Arabidopsis thaliana*, m^7G, m^6A, m^1A, m^5C, hm^5C, and uridylation have been identified as modifications in mRNA (Shen et al., 2019). The marriage between classical detection techniques and high-throughput sequencing has allowed to determine N^6-methyladenosine (m^6A) as the most prevalent chemical modification in mRNAs, both in animals and plants (Fray and Simpson, 2015). Transcriptome-wide analysis revealed that the m^6A mark in transcripts is predominantly localized near the stop codon and throughout the 3′ untranslated region (UTR) (Shen et al., 2019). An m^6A methylation motif (RR**A**CH [R = A/G; H = A/U/C; **A** = m^6A]) that is conserved between plants and other eukaryotic organisms has been described (Shen *et al.*, 2019). m^6A deposition, recognition and elimination are carried out by different proteins (Shen et al., 2019). Several cellular functions have been observed to be affected by m^6A modification, such as mRNA stability (Wei et al., 2018) or translational efficiency (Luo et al., 2014). In addition, proper m^6A deposition has been reported to be essential during *Arabidopsis* embryo development (Zhong et al., 2008) and to take part in biotic and abiotic plant stress responses (Martínez-Pérez et al., 2017; Anderson et al., 2018), fruit ripening (Zhou et al., 2019), flowering transition (Duan et al., 2017), leaf morphogenesis (Arribas-Hernández et al., 2018), trichome

development (Bodi et al., 2012) and apical shoot meristem development (Shen et al., 2016).

Nevertheless, little is known about the potential role of the epitranscriptome in the regulation of nitrogen (N) nutrition, with only the involvement of m^6A in the regulation of nitrate assimilation and signaling having been studied (Hou et al., 2021). However, N is an essential element for plant growth and development and a key component of cellular constituents such as nucleic acids, proteins, and chlorophylls (Hawkesford et al., 2012). In soils, plants can take up N inorganic forms such as nitrate (NO_3^-) or ammonium (NH_4^+) and organic forms such as urea, peptides, or amino acids (Jia and von Wirén, 2020). Plants such as rice, tea or maritime pine prefer NH_4^+ over NO_3^- as the main N source (Sasakawa and Yamamoto, 1978; Ruan et al., 2016; Ortigosa et al., 2020). In many plants, important changes in the transcriptome, proteome and metabolome have been described in relation to nitrogen nutrition and have mainly focused on the supply of NO_3^- and NH_4^+ (Patterson et al., 2010; Yang et al., 2018; Ravazzolo et al., 2020). In this way, it has been observed that these N forms trigger both shared and differential responses involving different pathways and many result in phenotypic differences such as specific changes in the root system architecture (RSA) and growth (Jia and von Wirén, 2020). Therefore, it is reasonable to hypothesize that some of these described responses to N nutrition may be influenced by epitranscriptome regulatory processes.

Oxford Nanopore Technology (ONT) is a third-generation sequencing platform that is currently the only option for direct sequencing of RNA samples without the requirement of reverse transcription and amplification steps (Parker et al., 2020). These characteristics are of great relevance in transcriptomics since they allow the reduction of sequencing biases and maintenance of nucleoside modifications that facilitate epitranscriptomics studies (Gao et al., 2021).

The aim of the present work is to shed light on the short-term response of maritime pine roots to NH_4^+ nutrition, elucidating what kind of regulatory relationship exists between transcriptomics, epitranscriptomics, proteomics and metabolite profiles. For this purpose, cutting edge and commonly used omics approaches, such as comprehensive transcriptome analyses by direct RNA sequencing (DRS) using Oxford Nanopore Technology (ONT), epitranscriptomic modification detection focused on m^6A assisted

by the ONT platform, and quantitative proteomic and metabolite profiling, were combined in the present study.

RESULTS

Metabolite profiling in response to NH_4^+ nutrition

Changes in the amounts of polar metabolites caused by short-term NH_4^+ nutrition were analyzed in maritime pine roots (Supplemental Dataset 1). A statistically significant decrease in the amounts of carbohydrates such as sucrose and glucose was observed (Figure 1; Supplemental Figure 1). Additionally, a statistically significant increase in shikimate levels was noted. In turn, although the results were not statistically significant, there was a slight trend of increased levels of glycolysis intermediary metabolites such as glucose-6 phosphate and glucose-1 phosphate as well as TCA anaplerotic pathway intermediates such as cis-aconitate and GABA. In parallel, an increase in the accumulation of L-glutamine, L-glutamate, and L-methionine, as well as in aromatic amino acids (L-phenylalanine and L-tryptophan), was observed in NH_4^+-treated plants. In contrast, metabolites such as L-asparagine, isocitrate, 2-oxoglutarate and L-malate were observed to decrease.

Direct RNA sequencing (DRS)

The global sequencing results are shown in Supplemental Table 1. The mean read sizes were between 908 bp to 1059 bp (Figure 2A). The longest reads ranged from 10298 bp to 14299 bp. Differential expression analyses identified 350 differentially expressed (DE) transcripts. From the total DE transcripts obtained, 106 were upregulated and 244 were downregulated (Figure 2B; Supplemental Dataset 2). Singular enrichment analysis (SEA) was performed individually for each gene expression regulation (up- and downregulated) to classify the biological functions under NH_4^+ nutrition. The SEA global results are shown in Supplemental Dataset 3. Upregulated transcripts were significantly enriched with GO terms for Biological Process (BP) such as “ammonia assimilation cycle” (GO:0019676), “protein glutathionylation” (GO:0010731), “response to cadmium ion” (GO:0046686) and “developmental growth” (GO:0048589); for Cellular Component (CC) such as “chloroplast stroma” (GO:0009570) and “cytosolic ribosome” (GO:0022626); and for Molecular Function (MF) such as “glutamate synthase (NADH) activity” (GO:0016040), “acylglycerol lipase activity” (GO:0047372) and “phospholipase activity” (GO:0004620) (Figure 2C; Supplemental Figure 2). The downregulated transcripts were enriched in the BP terms “response to

heat" (GO:0009408), "response to water deprivation" (GO:0009414), "protein folding" (GO:0006457) and "ethylene-activated signaling pathway" (GO:0009873) and the MF terms "calcium ion binding" (GO:0005509), "transcription coactivator activity" (GO:0003713), "mRNA binding" (GO:0003729), "chaperone binding" (GO:0051087) and "transcription factor activity, sequence-specific DNA binding" (GO:0003700). A more detailed study of the upregulated transcriptomic response revealed that *PpGS1b* (pp_68481) and *PpNADH-GOGAT* (pp_238920) were upregulated. Interestingly, transcripts for genes involved in defense-related response were upregulated: *PpAMP1* (pp_58005, pp_58008), different class IV chitinases (pp_239593, pp_239598, pp_239600, pp_117809), different splicing coding forms of patatin-like protein 2 (pp_71017, pp_71018, pp_71019, pp_71020, pp_71022), a PR-1 pathogenesis-related protein (pp_87427), a defensin coding transcript (pp_92119) and an RPW8 domain-containing protein (pp_142311) (Supplemental Dataset 2). Cell wall-related transcripts were also upregulated, such as those encoding expansin-A18 (pp_134987), nonclassical arabinogalactan protein 30 (pp_66323), probable prolyl 4-hydroxylase 4 (pp_235715), xyloglucan:xyloglucosyl transferase (pp_68519) and different forms of xyloglucan endotransglucosylase/hydrolase (pp_66707, pp_66708, pp_68517), was also observed. In contrast, the downregulation of different transcription factors (TFs) was observed (Supplemental Dataset 2), such as ethylene response factors (ERFs) (pp_58625, pp_58626, pp_86737, pp_96228, pp_96234), a trihelix transcription factor (pp_59947), and a MYB coding transcript (pp_202778). The repression of different splicing forms of an auxin-repressed protein/dormancy-auxin associated protein coding transcript (pp_58457, pp_58458, pp_58459, pp_58461, pp_58462, pp_58463), the SnRK1 regulator FCS-like zinc finger transcript (pp_202096), and transcripts encoding carbohydrate metabolism enzymes such as pyruvate decarboxylase (pp_78343, pp_123611, pp_126347) and sucrose synthase (pp_144843) was also observed. The differential expressions observed in DRS was confirmed by RT-qPCR analyses of seven transcripts including *SAM synthase, MYB5, PFK, AMP1, NADH-GOGAT, GS1b,* and *ASPG*. The results showed the same trend between the DRS and RT-qPCR results for all DE transcripts, with some differences in the logFC values (Figure 2D).

Differential DRS epitranscriptomics

To determine the differential epitranscriptomic marks, DRS results were explored to identify the chemically modified nucleosides in the mRNAs using Tombo software. After analysis, 513 statistically significant putative modified nucleosides were obtained in 283 transcripts (Figure 3A; Supplemental Dataset 4). There were 221 undermodified positions in 161 transcripts and 292 overmodified positions in 184 transcripts. Among them, 58 transcripts had significant over- and undermodified positions, including *PpGS1b* (pp_68474) and *translationally-controlled tumor protein* (*TCTP*, pp_72505) (Supplemental Dataset 5). The percentage of modifications for each kind of nucleoside was similar for adenosine, guanosine, and uridine (28%, 29% and 25%) but lower for cytidine (17%), without any obvious difference between sample conditions (Figure 3B). When the global set of modification ratios and transcript amounts were compared (Figure 3C), significant and negative correlations were found to be slightly stronger under NH_4^+ supply (-0.36) than under the control (-0.30) (Figure 3C). Modification ratios of individual nucleosides compared to transcript amounts were also similar (Supplemental Figure 3).

The functions of the transcripts with DE modifications were analyzed using SEA (Figure 3D; Supplemental Figure 4; Supplemental Dataset 6). A total of 116 significant GO terms were obtained. At the BP level, the main functions were related to the terms "ribosome biogenesis" (GO: 0042254); "translation" (GO:0006412), "proteolysis" (GO:0006508), "protein ubiquitination" (GO:0016567), "response to stress" (GO:0006950), "response to external biotic stimulus" (GO:0043207) and "glutamine metabolic process" (GO:0006541). Similarly, the "ribosome" term (GO:0005840) was the main function at the CC level. Finally, the terms "GTPase activity" (GO:0003924), "mRNA binding" (GO:0003729), "translation factor activity, RNA binding" (GO:0008135), "ubiquitin protein ligase binding" (GO:0031625), "ubiquitin conjugating enzyme activity" (GO:0061631) and "endopeptidase inhibitor activity" (GO:0004866) were the main functions at the MF level.

The differential modifications were verified using SELECT. This qPCR-based technique was initially designed to determine differential deposition of m^6A in total RNA mixtures. However, nucleoside modifications putatively detected in cytidine and uridine by Tombo were also detected with SELECT (Figure 3E). The obtained results

for each position showed a similar trend between the differential epitranscriptomic results from SELECT and Tombo (Figure 3E).

m^6A identification

The bioinformatic pipeline Nanom6A was used to specifically identify m^6A modifications in the RRACH sites from DRS data (Supplemental Dataset 7). The distribution of m^6A sites along the full-length transcripts showed a higher accumulation of marks over two-thirds of the relative length in control samples while a higher accumulation of marks in the final portion of the transcripts was observed in NH_4^+-treated samples (Figure 4A). A more detailed distribution study showed that m^6A sites were more abundant in the 5'-UTR and coding (CDS) regions under the control condition, while m^6A sites tended to be more abundant in the 3'-UTR regions of transcripts isolated from NH_4^+-treated seedlings (Figure 4B). The m^6A frequency was higher in the CDS, mainly in the central portion, and at the beginning of the 3'-UTR regions, but it was lower at the transcript ends (Figures 4A and 4B).

The most predominant RRACH sequence was AAACA (>15%), while GGACC was the least abundant (< 5%) (Figure 4C). The comparison between m^6A modification ratios and transcript amounts showed significant negative correlations for the control (-0.42) and NH_4^+ conditions (-0.46) (Figure 4D). The lengths of the poly(A) tails were determined from DRS data (Figure 4E). As expected, most of the poly(A) tails had a size between 40-250 nt with similar means in both conditions, 91.01 nt and 91.8 nt. The poly(A) tail lengths had significant positive correlations with m^6A ratios in both conditions (0.2) (Figure 4F). Significant but lower positive correlations were found when poly(A) tail lengths were compared with global and nucleoside modification ratios obtained with Tombo (Supplemental Figure 5). Finally, the poly(A) tail lengths and transcript amounts exhibited significant negative correlations for the control (-0.17) and NH_4^+ conditions (-0.18) (Figure 4G).

Differential proteomics

A total of 2,385 proteins were identified in the shotgun proteomics analysis (Supplemental Dataset 8). Among the identified proteins, 114 were differentially

regulated by NH_4^+: 38 were more abundant, while 76 were less represented (Figure 5A; Supplemental Dataset 8). To elucidate the biological roles of the identified proteins, SEA analyses were performed (Figure 5B; Supplemental Figure 6; Supplemental Dataset 9). The upregulated proteins showed as representative BP terms “cell redox homeostasis” (GO:0045454), “protein complex assembly” (GO:0006461), “translation” (GO:0006412), “cellular response to oxidative stress” (GO:0006979) and “defense response to bacterium” (GO:0042742). At CC level, “ribosome” (GO:0005840), “nucleolus” (GO:0005730) and “chloroplast” (GO:0009507) were the enriched terms. Finally, “structural constituent of ribosome” (GO:0003735) and “enzyme regulator activity” (GO:0030234) were the significant MF terms. Among the downregulated proteins, the representative enriched functions were “ribosome assembly” (GO:0042255), “ATP metabolic process” (GO:0046034), “translation” (GO:0006412), “response to metal ion” (GO:0010038) and “oxidation-reduction process” (GO:0055114) among the BP terms. At the CC level, the significant terms were “cytosol” (GO:0005829), “apoplast” (GO:0048046), “chloroplast” (GO:0009507) and “ribosome” (GO:0005840). “Oxidoreductase activity, acting on the aldehyde or oxo group of donors, NAD or NADP as acceptor” (GO:0016620), “structural constituent of ribosome” (GO:0003735), “GTPase activity” (GO:0003924) and “GTP binding” (GO:0005525) were the enriched MF terms.

The putative relationship between the m^6A modification ratio and protein abundance was determined through Pearson correlation analysis (Figure 5C). In NH_4^+-treated seedlings, a significant positive correlation was observed (0.18), while there was no correlation in control seedlings. The same effect was observed between nucleoside modification ratios from Tombo and protein amounts (Supplemental Figure 7). In addition, similar correlation results were obtained when poly(A) tail lengths and protein amounts were compared, and only NH_4^+-treated roots had a significant positive correlation (0.12) (Figure 5D).

Integration of data from omics approaches

The results of the different omics approaches employed in the present work were integrated to explore possible regulatory steps in response to NH_4^+ supply in maritime pine. The global results showed 30 different elements/genes with significant results

based on at least two approaches at least; 14 of them were significant in DRS and epitranscriptomics, 5 in DRS and proteomics, 9 in epitranscriptomics and proteomics, and 2 in all approaches (Figure 6A; Supplemental Dataset 10). Altogether, the genes/proteins identified were involved in N metabolism (*PpASPG*, *PpGS1b*, alanine-glyoxylate aminotransferase and isocitrate dehydrogenase), defense (*PpAMP1*, a ginkbilobin and a chitinase), oxidative stress response (alcohol dehydrogenase, aldehyde dehydrogenase, peroxidase and glutaredoxin), translation (ribosomal proteins and elongation factors) and RNA binding (cold shock proteins and a BURP domain protein RD22). Among them, the presence of the 1-aminocyclopropane-1-carboxylate (ACC) oxidase, which had a putative modification at the position 462 on the contig, must be highlighted. This epitranscriptomic mark was overexpressed (logFC 0.84) under NH_4^+ nutrition, while the ACC oxidase protein was underexpressed (logFC -2.69). Similarly, changes in transcript level, protein level and transcript modification ratio can show opposite trends with variations between genes. For the aldehyde dehydrogenase, the transcript expression and modification were overexpressed (0.58 and 0.73, respectively), but protein expression was underexpressed (logFC -1.20). However, for the CSP/GRP (pp_211512 and pp_211516), transcript accumulation was underexpressed (-0.43 and -0.7) and the epitranscriptomic modifications and protein expression were overexpressed (0.88-0.73 and 2.11 respectively).

The comparison between the significant GO terms in the omics approaches revealed that 94 of the 287 GO terms were shared (Figure 6B-6C; Supplemental Dataset 11). Interestingly, 20 (7%) of them were common to the three sets of results. The epitranscriptomics and proteomics comparison included the highest number of GO terms (59, 20.6%), and the transcriptomics and proteomics comparison included the lowest number, with only 5 (1.7%). The most representative GO terms common to the three omics datasets were “ribosome” (GO:0005840), “structural constituent of ribosome” (GO:0003735) and “translation” (GO:0006412). Between the transcriptomics and epitranscriptomics datasets, “mRNA binding” (GO:0003729) and “glutamine metabolic process” (GO:0006541) were the main GO terms. In the transcriptomics and proteomics comparison, “oxoacid metabolic process” (GO:0043436) was the main GO term. Finally, between epitranscriptomics and proteomics the main GO terms were “small ribosomal subunit” (GO:0015935), “GTPase activity” (GO:0003924), “ribosome

assembly” (GO:0042255), “defense response” (GO:0006952) and “response to external stimulus” (GO:0009605). According to these functional results, several transcripts coding for eukaryotic ribosomal proteins (38) and translation factors (8) had differential epitranscriptomic marks based on the Tombo results (Figure 6D).

DISCUSSION

The response of maritime pine roots to NH_4^+ nutrition has been studied from a multiomics perspective that includes direct RNA sequencing using the ONT platform, which has allowed a global epitranscriptomics analysis. Although N is an essential nutrient for proper plant growth and development (Xu et al., 2012), little is known about the role of epitranscriptomic marks in the regulation of gene expression in response to N nutrition. The results in the present work highlight the importance of epitranscriptomic marks in the regulation of gene expression.

Epitranscriptome changes in response to NH_4^+ nutrition

Correlation of global epitranscriptomics results with transcript abundance (Figure 3C), especially m^6A modifications (Figure 4D), are consistent with those from previous works in *Populus* (Gao et al., 2021) and *Arabidopsis* (Luo et al., 2014; Wan et al., 2015) and support the role of m^6A in mRNA decay, as previously described in mammals (Wang et al., 2014; Li et al., 2019). Additionally, m^6A identification revealed that in the roots of maritime pine, AAACA and AAACU were the most abundant RRACH 5-mer motifs (Figure 4C), as previously reported in *Arabidopsis*, maize, and poplar (Wan et al., 2015; Miao et al., 2020; Parker et al., 2020; Gao et al., 2021). These findings strongly suggest conservation of the RNA m^6A methylation machinery in plants. However, pine m^6A distribution, with similar levels of enrichment in the middle of the CDS and at beginning of the 3'-UTR (Figure 4A-4B), slightly differs from the obtained results in angiosperms, where a greater enrichment of m^6A was observed in the 3'-UTR (Miao et al., 2020; Parker et al., 2020; Gao et al., 2021). This discrepancy may be attributed to the lack of a well-curated reference genome for maritime pine. Interestingly, the distribution of m^6A sites in pine transcripts is dynamically regulated by increasing the m^6A deposition in the 3'-UTR in response to NH_4^+, which seems to be correlated with poly(A) length and changes in protein abundance (Figure 6C-6D), as well as the identification of transcripts with upregulated and downregulated epitranscriptomic marks (Supplemental Dataset 5). This observation agrees with previous results in other eukaryotic organisms (Meyer et al., 2012; Anderson et al., 2018).

A previous work in *Caenorhabditis elegans* reported that highly expressed transcripts contained a relatively short and well-defined poly(A) tail (Lima et al., 2017), which has been related to translational efficiency (Wu et al., 2020). Our results reveal that increased poly(A) tail lengths correlated with higher m^6A and lower transcript abundances (Figure 4F-4G). These findings are consistent with the effect of m^6A modifications on transcript levels (Figure 4D), which follow the same trend as previously published results (Luo et al., 2014; Wan et al., 2015; Parker et al., 2020; Gao et al., 2021). The integration of all these results with the positive correlations of m^6A ratios and poly(A) tail length with protein amounts (Figure 5C-5D) suggests that m^6A could affect in the translation efficiency of the differentially modified transcripts, as previously described in mammals (Meyer, 2019). This evidence could also explain, at least in part, the lack of a relationship between the transcriptomic, proteomic and metabolite data.

Epitranscriptomic marks, mainly m^6A, seem to modulate protein synthesis through mRNA stability and modify the translation processes. This is in line with a previous hypothesis considering that initial gene responses caused by environmental factors are modulated at the level of final products of gene expression to maintain cellular homeostasis (Cañas et al., 2015). Thus, the variable transcriptomic response can be controlled through intermediate steps, such as epitranscriptomic regulation, to generate an appropriate and stable cellular response.

Carbon and nitrogen metabolism

As expected, N assimilation was induced by NH_4^+, as shown by the significant increase in *GS1b* and *NADH-GOGAT* transcripts and the concomitant accumulation of L-glutamine and L-glutamate (Figure 1 and 7; Supplemental Dataset 3), consistent with previous transcriptomic reports (Li et al., 2017; Sun et al., 2017). However, no upregulation of GS1b and NADH-GOGAT was observed at the proteomic level (Supplemental Dataset 8), even though a trend towards higher GS activity was observed in the presence of NH_4^+ (Supplemental Figure 8). Similar proteomics results for NH_4^+ nutrition have been described before (Marino et al., 2016; Coleto et al., 2019), as well as the lack of correlation between relative expression levels of GS transcripts and GS activity. To explain these discrepancies, it was hypothesized that the response to N

nutrition could be regulated through a posttranscriptional (translational or posttranslational) mechanism (Ortigosa et al., 2020). In this way, several nucleosides with differential epitranscriptomic marks, including m^6A, have been identified in *GS1b* transcripts, which could explain the differences between transcriptomics and proteomics data (Supplemental Dataset 4 and 7). Accordingly, in *Arabidopsis*, m^6A can regulate the alternative polyadenylation and transcript abundance of the *GLN1;1* and *GLN1;3* genes during nitrate assimilation and signaling (Hou et al., 2021).

Additionally, the results of this study suggest the existence of a carbon flux through glycolysis and the TCA cycle to provide carbon skeletons for N assimilation (de la Peña et al., 2019). Interestingly, the fermentation pathway seems to be repressed, as suggested by the downregulation of pyruvate decarboxylase (PDC) transcripts and the decrease in alcohol dehydrogenase (ADH) and aldehyde dehydrogenase (ALDH) protein levels (Supplemental Datasets 2 and 7). It is well known that plants under low oxygen conditions regulate their metabolism, inducing the fermentation pathway in which PDC and ADH activities are essential, which results in pyruvate consumption, the production of ethanol and the concomitant oxidation of NADH to NAD^+ (Mithran et al., 2014). The repression of the fermentative pathway and the overrepresentation of TIM proteins (inner membrane translocase proteins) (Supplemental Dataset 7) highlight the need for organic acids to assimilate NH_4^+ and produce energy for plant growth.

Defense response

Nitrogen status is often related to plant disease emergence and plant immunity (Fagard et al., 2014). It is well known that NH_4^+ induces the upregulation of defense-related genes *in planta* (Ravazzolo et al., 2020). The results presented here demonstrate the transcriptional activation of defense-related genes, such as those encoding for class IV chitinase, defensin 5.1, beta-lactamase and a thaumatin-like protein, in maritime pine roots in response to the NH_4^+ supply (Supplemental Dataset 2). A similar tendency was observed at the proteomic level for several ginkbilobin antifungal proteins (Wang and Ng, 2000). This effect highlights the importance of the upregulation of this kind of genes in conifers in their natural environment since these plants have adapted to living in suboptimal environments where nutrient availability is a limiting factor for their growth and development (Farjon, 2018).

In this context, the upregulation of *antimicrobial peptide 1* and *pathogenesis-related protein PR-1* transcripts was consistent with previous results in maritime pine roots (Canales et al., 2010). Pine AMP1 is known to inhibit fungal development (Canales et al., 2011). It has been proposed that, related to its defensive function, AMP1 can inhibit the NH_4^+ uptake in maritime pine, possibly through a physical interaction with ammonium transporters (AMT) (Castro-Rodríguez et al., 2017). Additionally, related to AMT activity regulation, transcriptomic results showed a wide repression of several transcripts coding for *calcineurin B-like* (*CBL)-interacting protein kinases* and *calcium-binding proteins* (Supplemental Dataset 2); in the second case, the transcript also contained significant modifications (Supplemental Dataset 10). The protein kinase CIPK23 has been shown to phosphorylate T460 of AtAMT1.1 and AtAMT1.2 in a CBL-1-dependent manner, repressing NH_4^+ transport (Straub et al., 2017). These results imply transcriptional regulation of NH_4^+ uptake resulting in proper N acquisition and assimilation. However, no statistically significant changes in the AMT proteins were observed, likely due to the relevance of their posttranslational regulation (Figure 3; Supplemental Dataset 2).

Ethylene

Transcriptomic studies carried out in rice described that under excess NH_4^+, ethylene (ET) could be one of the major regulatory molecules in roots (Sun et al., 2017). Additionally, Li et al. (2013) described in *Arabidopsis* that shoot-supplied NH_4^+ promoted ET biosynthesis only in shoots, resulting in a reduction in the lateral root formation process due to *auxin transporter 1* (*AUX1*) repression. These data might indicate that ET biosynthesis is involved in detrimental NH_4^+-related phenotypes, such as a reduction in the number of lateral roots (LRs). Some reports have described that the application of inhibitors of the ET biosynthesis improved symptoms of NH_4^+ toxicity affecting RSA (Li et al., 2013). However, previous results indicated that NH_4^+ promotes root growth in maritime pine seedlings (Ortigosa et al., 2020).

A comparison of the root transcriptomic response and differential proteomics results revealed that NH_4^+ promotes a decrease in ET-related transcripts and proteins. Several ET-responsive TFs were downregulated at the transcriptomic level, while proteomic results revealed that ACC oxidase was downregulated (Supplemental Datasets 2 and 7).

ACC oxidase is the enzyme responsible for the final stage in the biosynthesis of ET in plants (John et al., 1999). Furthermore, ACC oxidase transcripts exhibited a nucleoside putative modification in the 3'-UTR (position 462) that was differentially increased under NH_4^+ treatment (Supplemental Dataset 10). Since the levels of ACC oxidase transcripts had no significant changes, it is possible that this epitranscriptomic mark could be involved in the translational regulation of these transcripts, therefore affecting the ET levels of the organ. Interestingly, it is reasonable to think that this kind of response could be based on conifer preference for NH_4^+. Additional technical approaches are required to identify the exact modification and validate its biological relevance in the regulation of ACC oxidase and ET synthesis. Finally, the relationship between ET and N nutrition is remarked by the differential expression (negative) of a trihelix family TF that has a very high similarity degree to *AT3G54390* in *Arabidopsis* (Figure 7). This TF in *Arabidopsis* can interact with the promoters of genes involved in N metabolism and ET biosynthesis including *glutamine synthetase* (AT1G66200), *nitrite reductase* (AT2G15620), *ET-responsive transcription factor* (*ERF012*; AT1G21910) and *1-aminocyclopropane-1-carboxylate synthase* (AT5G65800) (Gaudinier et al., 2018).

Translation and growth

The results also indicate a reconfiguration of the ribosomal proteins and elongation factors at all biological levels, although this was more visible in epitranscriptomics and proteomics results (Figure 6D and 7; Supplemental Datasets 2, 4, 7 and 10). This process is clearly related to the correlation between m^6A ratios and protein amounts (Figure 5C), suggesting that NH_4^+ nutrition promotes general translation activation to support the root growth of maritime pine seedlings. This kind of effect on the ribosomal protein composition and proteins involved in translation has been previously observed under different conditions, including plant mineral nutrition (Wang et al., 2013; Prinsi and Espen, 2018; Ferretti and Karbstein, 2019). The data suggest that changes in the profiles of ribosomal proteins can be significantly mediated by epitranscriptomic modifications to their transcripts. These posttranscriptional changes can influence ribosome function and performance. One example is the RACK1 proteins, which are components of the small subunit of the ribosome and are involved in translation quality

control promoting the endonucleolytic cleavage of nonstop mRNA (Ikeuchi and Inada, 2016). Interestingly, the mRNA of a *RACK1* gene in maritime pine roots has several differential epitranscriptomic marks (Supplemental Datasets 4 and 5). Although it was not significant, RACK1 protein expression was repressed under NH_4^+ conditions, suggesting a change in the quality control mechanisms and even in the integration of the plant signaling pathways. These proteins in plants are involved in the response to phytohormones, including ET, and in the regulation of growth and development (Wang et al., 2019). This result agrees with the negative regulation of ACC oxidase and repression of several ET-responsive factors (Supplemental Datasets 2 and 7). Accordingly, ET signaling affects gene translation in different ways (Merchante et al., 2015).

Additionally, related to the regulation of translation and root growth, among the transcriptomic results, the repression of an *FCS-like zinc finger* was observed (Supplemental Dataset 2). FCS proteins interact with SnRK1 to mediate the interaction of SnRK1 with other proteins (Jamsheer et al., 2018). SnRK1 is a kinase that phosphorylates RAPTOR, a regulatory element of the TOR complex, repressing TOR activity (Fu et al., 2020). Considering the ribosomal protein changes and the increase in root growth under NH_4^+ nutrition in maritime pine seedlings (Ortigosa et al., 2020), it can be hypothesized a decrease of SnRK1 activity over the TOR complex in these conditions. The TOR complex integrates different developmental and environmental signals, including nutritional status, promoting ribosome biogenesis, translation, and plant growth.

Finally, a transcript coding for a TCTP protein had several differential modifications (Supplemental Dataset 5). It is well established in plants that *TCTP* mRNA is synthetized in shoots and transported to roots, where it is translated and promotes lateral root formation (Branco and Masle, 2019). Interestingly, transport of this mRNA is mediated through epitranscriptomic marks (Yang et al., 2019). This suggests additional mechanisms controlling growth and development in response to N nutrition in maritime pine roots.

Therefore, the results presented in this work suggest that protein translation and growth are finely regulated through epitranscriptomic marks, including m^6A, to acquire an optimum response to N supply (Figure 7). More research efforts are required to

corroborate this hypothesis and to investigate whether ET could act as a modulator of the integrated response observed due to its effects on the translation process.

MATERIALS AND METHODS

Plant material

Seeds from maritime pine (*Pinus pinaster* Ait.) from "Sierra Segura y Alcaraz" (Albacete, Spain) were provided by from the *Área de Recursos Genéticos Forestales* of the Spanish *Ministerio de Agricultura, Pesca y Alimentación*. Maritime pine seed germination was carried out following the protocol described in (Cañas et al., 2006). Seedlings were grown in vermiculite in plant growth chambers under 16 h light photoperiod, a light intensity of 100 $\mu mol\ m^{-2}\ s^{-1}$, constant temperature of 25 °C and watered twice a week with distilled water. One-month old maritime pine seedlings were used for this experiment. Pine seedlings were randomly subdivided into two different groups, relocated into forestall seedbeds and watered with 80 mL distilled water. After three days of acclimation, the control group was irrigated with 80 mL of water (C) and the experimental group with 80 mL of 3 mM NH_4Cl. Root samples were collected at 24 hours post-irrigation and immediately frozen in liquid N. This experiment was carried out three independent times. The adequate development of each experiment was verified through the gene expression analysis by RT-qPCR of two control genes, *PpAMT1.3* and *PpAMP1* following previous results (Canales et al., 2011; Castro-Rodríguez et al., 2016).

Metabolite profile

The metabolites for ^{1}H-NMR analysis were extracted following the protocol previously described by Kruger et al. (2008). Two hundred milligrams of frozen powder were used for extractions. The ^{1}H-NMR analyses were performed on an ASCEND 400 MHz NMR Spectrometer (Bruker, Billerica, MA, USA) in the Bionand Centre (Malaga, Spain). The 1D-^{1}H-NMR spectrum for each sample was obtained as previously described by Cañas et al. (2015). Quantitative analysis of the NMR spectra was performed using LCModel software (Provencher, 1993) and a previously generated reference metabolite spectral library (Cañas et al., 2015). The internal reference was an electronically generated signal, ERETIC (Akoka et al., 1999). The metabolite amounts were determined at millimolar concentrations. The metabolite contents were analyzed with MetaboAnalyst 4.0 (Chong et al., 2018). Data were normalized using the quantile method, then log transformation and mean centered. MetaboAnalyst 4.0 was used to construct a Heatmap and perform a t-test with the metabolite data.

Total RNA isolation

Total root RNA from maritime pine seedlings was isolated following the protocol described by Liao et al. (2004) and modified by Canales et al. (2012). The RNA concentration and purity were determined *via* spectrophotometry on a Nanodrop ND-1000 (Thermo Scientific, Waltham, MA, USA). Purity was determined through the 260/280 and 260/230 ratios. RNA quality was also determined in a Bioanalyzer 2100 (Agilent, Santa Clara, CA, USA). The concentration was verified with a Qubit 4 Fluorometer (Invitrogen, Paisley, UK) and Qubit RNA BR, Broad-Range, Assay Kit (Invitrogen, Paisley, UK).

mRNA isolation and preparation

Samples with a RIN value > 7 were selected to mRNA isolation. The poly(A)-RNA isolation was performed using Dynabeads™ mRNA Purification Kit (Invitrogen, Paisley, UK) following the manufacturer's instructions. This process was carried out twice per sample to avoid rRNA contamination. poly(A)-RNA quality was determined in a Bioanalyzer 2100 (Agilent, Santa Clara, CA, USA). The concentration was verified with a Qubit 4 Fluorometer (Invitrogen, Paisley, UK) and Qubit RNA HS, High Sensitivity, Assay Kit (Invitrogen, Paisley, UK).

Direct RNA sequencing (DRS) and differential epitranscriptomic analysis

Nanopore libraries for DRS were prepared from 1.65 up to 2.18 µg of isolated poly(A)-RNA using the Nanopore Direct RNA Sequencing kit (SQK-RNA001, Oxford Nanopore Technologies, ONT, Oxford, UK) according to manufacturer's instructions. The DRS libraries were loaded onto a R9.4 SpotON Flow Cells (Oxford Nanopore Technologies, Oxford, UK) and sequenced until complete nanopores depletion. Extended method descriptions are in the Supplemental Methods 1. Basecalling was carried out with ONT Guppy software (https://community.nanoporetech.com). The resultant reads were filtered by quality (Q>9). Read alignment was made with minimap2 software (Li, 2018) using root transcriptome of maritime pine as reference. The alignment parameters were adjusted for DRS (*-uf* and *-k14*). Differentially expressed (DE) transcripts were identified using the edgeR package for R, the transcripts were normalised by count per million mapped reads (cpm) and filtered (2

cpm in at least 2 samples) (Robinson et al., 2010). The transcripts with False Discovery Rate < 0.05 (FDR < 0.05) were considered as differentially expressed.

ONT-DRS reads were used for *de novo* modification detection with the TOMBO software (Stoiber et al., 2017). The total mapped reads per base and the number of modified bases in each position were obtained using the *text_output_browser_file* method with the options *coverage* and *fraction*. Only the positions with at least 50 mapped reads were employed for subsequent analyses. A Fischer exact test was carried out for each transcript position to determine the differential expression of modified bases among control and NH_4^+ supplied samples. The transcript positions with a *P*-value < 0.05 and an absolute logFC > 0.5 were considered as differentially modified.

Transdecoder software (https://github.com/TransDecoder/transdecoder.github.io) were used to determine modification positions and nucleobases in the transcripts of the reference transcriptome. Identification of m^6A sites were carried out with the bioinformatic pipeline *Nanom6A* using default parameters (Gao et al., 2021). The length of poly(A) tails were determined using *Nanopolish* 0.11.1 software package (https://github.com/adbailey4/nanopolish) with the *polya* function.

Functional annotation and enrichment analyses

The transcriptome was functional annotated with BLAST2GO (Götz et al., 2008) using DIAMOND software with *blastx* option (Buchfink et al., 2015) result against the NCBI's plants-*nr* database (NCBI Resource Coordinators, 2016). Blast results were considered valid with e-value < 1.0E-6. Singular enrichment analysis (SEA) of the GO terms was made in the AGRIGO v2.0 web tool under standard parameters using as GO term reference the whole assembled transcriptome annotation (Tian et al., 2017). Representative enriched GO was determined using REVIGO (Supek et al., 2011).

RT-qPCR

The cDNA synthesis was performed using 1 µg of total RNA and iScript™ cDNA Synthesis Kit (Bio-Rad, Hercules, CA, USA) following manufacturer's instructions. The qPCR primers were designed following the MIQE guidelines (Bustin *et al.*, 2009). The primers are listed in the Supplemental Table 2. qPCRs were carried out using 10 ng of cDNA and 0.4 mM of primers and 2X SsoFast™ EvaGreen® Supermix (Bio-Rad, Hercules, CA, USA) in a total volume of 10 µL. Relative quantification of gene expression was performed using thermocycler CFX 384™ Real-Time System, Bio-Rad,

Hercules, CA, USA). The qPCR program was: 3 min at 95 °C (1 cycle), 1 s at 95 °C and 5 s at 60 °C (50 cycles) and a melting curve from 60 to 95 °C, to generate the dissociation curve in order to confirm the specific amplification of each individual reaction. The analyses were carried out as described by Cañas et al. (2014) using the MAK3 model in the R package *qpcR* (Ritz and Spiess, 2008). Expression data were normalized to two reference genes, SKP1/ASK1 and SLAP that were previously tested for RT-qPCR experiments in maritime pine (Granados et al., 2016). The qPCR analyses were made with three biological replicates and three technical replicates per sample.

Validation of differential deposition of m^6A by RT-qPCR

The validation of the differential deposition of m^6A in the transcripts were made using the SELECT method (Xiao et al., 2018). A differential cDNA synthesis was made per each transcript with 30 ng of total RNA. qPCR determinations were made with 2 µL of cDNA. The expression level of each transcript was determined in parallel by RT-qPCR and their result were used to normalize the SELECT results. The primers are listed in the Supplemental Table 2. Extended method description can be found in the Supplemental Methods 1.

Differential proteomics analysis

The proteins were extracted following the protocol described by González Fernández et al. (2014). The extractions were carried out with 200 mg of sample. Protein content was determined using a commercially kit (Protein Assay Dye Reagent; Bio-Rad, CA, USA) and bovine serum albumin as a standard (Bradford, 1976). Protein extracts were cleaned-up in 1D SDS-PAGE at 10% polyacrilamyde as described in Valledor and Weckwerth, 2014. Protein bands were cut off, diced, and kept in water at 4ºC until digestion.

Protein digestion and nLC-MS2 analysis were carried out in the Proteomics Facility at Research Support Central Service, University of Cordoba. Nano-LC was performed in a Dionex Ultimate 3000 nano UPLC (Thermo Scientific, Waltham, MA, USA) with a C18 75 µm x 50 Acclaim Pepmam column (Thermo Scientific, Waltham, MA, USA). Eluting peptide cations were converted to gas-phase ions by nano electrospray ionization and analyzed on a Thermo Orbitrap Fusion (Q-OT-qIT, Thermo Scientific) mass spectrometer operated in positive mode. Extended method descriptions are in the Supplemental Methods 1.

Root transcriptome from *Pinus pinaster* was translated into the six open reading frames with *transeq* tool (Madeira et al., 2019). The output peptides chains were filtered by length, deleting those less than 50 amino acids (Romero-Rodríguez et al., 2014). To reduce the redundancy of proteins in the database, CD-HIT-EST with a 99% identity filter was used (Fu et al., 2012). The raw data were processed using Proteome Discoverer (version 2.3, Thermo Scientific). MS2 spectra were searched with SEQUEST engine against the reference proteome database. *In silico* peptide lists were created using the followings settings: trypsin digestion, a maximum of two missed internal cleavage sites per peptide, precursor mass tolerance of 10 ppm and fragment mass tolerance of 0.75 Da per fragment ions. Only peptides with a high confidence (FDR $\leq$ 0.01) and minimum XCorr of 2 were selected. The identified proteins were filtered by a minimum of two different peptides. *Minora* algorithm was used to determine relative quantification. The protein identification with redundancy is considered by Proteome Discoverer and SEQUEST software. Proteins sharing peptides were grouped and all those groups without a unique peptide were removed. Only proteins detected in 5 of the 6 samples were considered for subsequent analyses. The resultant proteins were annotated using BLAST with *blastp* option against NCBI's non-redundant database (Camacho et al., 2008) and BLAST2GO software (Götz et al., 2008). Proteins with the same sequence annotation and quantification profile across the samples was considered the same protein selecting the protein with the longest sequence. Normalized data from Proteome Discoverer software were used for a differential expression analysis using the edgeR package for R (Robinson et al., 2010). Only the proteins with *P*-value < 0.05 were considered as differentially expressed.

Accession Numbers

The sequences of genes examined in this study can be found in Genbank under the following accession numbers: KC807909 (*PpAMT1.3*) and HM210085 (*PpAMP1*). The root transcriptome sequences consulted at https://fmp.uma.es/sequenceserver/ or can also be obtained on demand from the contact author. The DRS data have been deposited in the NCBI's Gene Expression Omnibus (Edgar et al., 2002) and are accessible through GEO Series with the accession number GSEXXX (uploading). The mass spectrometry proteomics data have been deposited to the ProteomeXchange Consortium via the PRIDE partner repository (Vizcaino et al., 2013) with the dataset identifier PXD025331 and 10.6019/PXD025331.

AUTHOR CONTRIBUTIONS

F.O. have performed the experiments; C.L.F. has performed the bioinformatic analyses; J.P.C. and F.R.C. have performed the statistical data analysis; F.O. and R.A.C. have wrote the manuscript; C.A. and F.M.C. made additional contributions and edited the manuscript. F.O. and R.A.C. have planned and designed the research. R.A.C, C.A.V., and F.M.C were the responsible of the funding acquisition.

ACKNOWLEDGEMENTS

This work was funded by Spanish *Ministerio de Economía y Competitividad*, grants numbers BIO2015-73512-JIN MINECO/AEI/FEDER, UE, BIO2015-69285-R and RTI2018-094041-B-I00. FO was partially supported by a grant from the *Universidad de Málaga* (*Programa Operativo de Empleo Juvenil vía SNJG, UMAJI11, FEDER, FSE, Junta de Andalucía*).

REFERENCES

Akoka, S., Barantin, L., and Trierweiler, M. (1999). Concentration measurement by proton NMR using the ERETIC method. Analytical Chemistry, 71: 2554-2557, https://doi.org/10.1021/ac981422i.

Anderson, S.J., Kramer, M.C., Gosai, S.J., Yu, X., Vandivier, L.E., Nelson., A.D., Anderson, Z.D., Beilstein, M.A., Fray, R.G., Lyon, E., and Gregory, B.D. (2018). N^6-methyladenosine inhibits local ribonucleolytic cleavage to stabilize mRNAs in *Arabidopsis*. Cell Reports, 25: 1146-1157, https://doi.org/10.1016/j.celrep.2018.10.020.

Arribas-Hernández, L., Bressendorff, S., Hansen, M.H., Poulsen, C., Erdmann, S., and Brodersen, P. (2018). An m^6A-YTH module controls developmental timing and morphogenesis in *Arabidopsis*. The Plant Cell, 30: 952-967, DOI: https://doi.org/10.1105/tpc.17.00833.

Bodi, Z., Zhong, S., Mehra, S., Song, J., Graham, N., Li, H., May, S., and Fray, R.G. (2012). Adenosine methylation in *Arabidopsis* mRNA is associated with the 3' end and reduced levels cause developmental defects. Frontier in Plant Science, 3: 48, https://doi.org/10.3389/fpls.2012.00048.

Bradford, M.M. (1976). A rapid and sensitive method for the quantitation of microgram quantities of protein utilizing the principle of protein-dye binding. Analytical Biochemistry, 72: 248-254, https://doi.org/10.1006/abio.1976.9999.

Branco, R., and Masle, J. (2019). Systemic signalling through translationally controlled tumour protein controls lateral root formation in *Arabidopsis*. Journal of Experimental Botany, 70: 3927-3940, https://doi.org/10.1093/jxb/erz204.

Buchfink, B., Xie, C., and Huson, D.H. (2015). Fast and sensitive protein alignment using DIAMOND. Nature Methods, 12: 59-60, https://doi.org/10.1038/nmeth.3176.

Bustin, S.A., Benes, V., Garson, J.A., Hellemans, J., Huggett, J., Kubista, M., Mueller, R., Nolan, T., *et al*. (2009). The MIQE guidelines: minimum information for publication of quantitative real-time PCR experiments. Clinical Chemistry, 55: 611-622, https://doi.org/10.1373/clinchem.2008.112797.

Camacho, C., Coulouris, G., Avagyan, V., Ma, N., Papadopoulos, J., Bealer, K., and Madden, T.L. (2008). BLAST+: architecture and applications. BMC Bioinformatics, 10: 421, https://doi.org/10.1186/1471-2105-10-421.

Canales, J., Flores-Monterrosso, A., Rueda-López, M., Avila, C., and Cánovas, F.M. (2010). Identification of genes regulated by ammonium availability in the roots of maritime pine trees. Amino Acids, 39: 991-1001, https://doi.org/10.1007/s00726-010-0483-9.

Canales, J., Avila, C., and Canovas, F.M. (2011). A maritime pine antimicrobial peptide involved in ammonium nutrition. Plant, Cell & Environment, 34: 1443-1453, https://doi.org/10.1111/j.1365-3040.2011.02343.x.

Canales, J., Rueda-López, M., Craven-Bartle, B., Avila, C., and Cánovas, F.M. (2012). Novel insights into regulation of asparagine synthetase in conifers. Frontiers in Plant Science, 3: 100, https://doi.org/10.3389/fpls.2012.00100.

Cañas, R.A., de la Torre, F., Cánovas, F.M., and Cantón, F.R. (2006). High levels of asparagine synthetase in hypocotyls of pine seedlings suggest a role of the enzyme in re-allocation of seed-stored nitrogen. Planta, 224: 83-95, https://doi.org/10.1007/s00425-005-0196-6.

Cañas, R. A., Canales, J., Gómez-Maldonado, J., Ávila, C., & Cánovas, F. M. (2014). Transcriptome analysis in maritime pine using laser capture microdissection and 454 pyrosequencing. Tree Physiology, 34: 1278-1288, https://doi.org/10.1093/treephys/tpt113.

Cañas, R.A., Canales, J., Muñoz-Hernández, C., Granados, J.M., Ávila, C., García-Martín, M.L., and Cánovas, F.M. (2015). Understanding developmental and adaptive cues in pine through metabolite profiling and co-expression network analysis. Journal of Experimental Botany, 66: 3113-3127, https://doi.org/10.1093/jxb/erv118.

Castro-Rodríguez, V., Assaf-Casals, I., Pérez-Tienda, J., Fan, X., Avila, C., Miller, A., and Cánovas, F.M. (2016). Deciphering the molecular basis of ammonium uptake and transport in maritime pine. Plant, Cell & Environment, 39: 1669-1682, https://doi.org/10.1111/pce.12692.

Castro-Rodríguez, V., Cañas, R.A., de la Torre, F.N., Pascual, M.B., Avila, C., and Cánovas, F.M. (2017). Molecular fundamentals of nitrogen uptake and transport in trees. Journal of Experimental Botany 68: 2489-2500, https://doi.org/10.1093/jxb/erx037.

Chong, J., Soufan, O., Li, C., Caraus, I., Li, S., Bourque, G., Wishart, D., and Xia, J. (2018). MetaboAnalyst 4.0: towards more transparent and integrative metabolomics analysis. Nucleic Acids Research, 46: 486-494, https://doi.org/10.1093/nar/gky310.

Coleto, I., Vega-Mas, I., Glauser, G., González-Moro, M.B., Marino, D., and Ariz, I. (2019). New insights on *Arabidopsis thaliana* root adaption to ammonium nutrition by the use of a quantitative proteomic approach. International Journal of Molecular Sciences, 20: 814, https://doi.org/10.3390/ijms20040814.

Crick, F. (1970). Central dogma of molecular biology. Nature, 227:561-563, https://doi.org/10.1038/227561a0.

de la Peña, M., González-Moro, M.B., and Marino, D. (2019). Providing carbon skeletons to sustain amide synthesis in roots underlines the suitability of *Brachypodium distachyon* for the study of ammonium stress in cereals. AoB Plants, **11:** plz029, https://doi.org/10.1093/aobpla/plz029.

Duan, H.C., Wei, L.H., Zhang, C., Wang, Y., Chen, L., Lu, Z., Chen, P.R., He, C., and Jia, G. (2017). ALKBH10B is an RNA N^6-methyladenosine demethylase affecting *Arabidopsis* floral transition. The Plant Cell, 29:2995–3011, https://doi.org/10.1105/tpc.16.00912.

Edgar, R., Domrachev, M., and Lash, A.E. (2002). Gene Expression Omnibus: NCBI gene expression and hybridization array data repository. Nucleic Acids Research**,** 30: 207-210, https://doi.org/10.1093/nar/30.1.207.

Fagard, M., Launay, A., Clément, G., Courtial, J., Dellagi, A., Farjad, M., Krapp, A., Soulié, M.C., and Masclaux-Daubresse, C. (2014). Nitrogen metabolism meets phytopathology. Journal of Experimental Botany, 65:5643-5656, https://doi.org/10.1093/jxb/eru323.

Farjon, A. (2018). The Kew review: conifers of the world. Kew Bulletin, 73: 8.

Ferretti, M.B., and Karbstein, K. (2019). Does functional specialization of ribosomes really exist? RNA, 25**:** 521-538, https://doi.org 10.1261/rna.069823.118.

Fray, R.G., and Simpson, G.G. (2015). The Arabidopsis epitranscriptome. Current Opinion in Plant Biology, 27: 17-21, https://doi.org/10.1016/j.pbi.2015.05.015.

Fu, L., Niu, B., Zhu, Z., Wu, S., and Li, W. (2012). CD-HIT: accelerated for clustering the next generation sequencing data. Bioinformatics. 28: 3150-3152, https://doi.org/10.1093/bioinformatics/bts565.

Fu, L., Wang, P., and Xiong, Y. (2020). Target of rapamycin signaling in plant stress responses. Plant Physiology, 182**:** 1613-1623, https://doi.org/10.1104/pp.19.01214.

Gao, Y., Liu, X., Wu, B., Wang, H., Xi, F., Kohnen, M.V., Reddy, A.S.N., and Gu, L. (2021). Quantitative profiling of N^6-methyladenosine at single-base resolution in stem-differentiating xylem of *Populus trichocarpa* using Nanopore direct RNA sequencing. Genome Biology, 22: 22, https://doi.org/10.1186/s13059-020-02241-7.

Gaudinier, A., Rodriguez-Medina, J., Zhang, L., Olson, A., Liseron-Monfils, C., Bågman, A. M., Foret, J., Abbitt, S., *et al.* (2018). Transcriptional regulation of nitrogen-associated metabolism and growth. Nature, 563: 259–264, https://doi.org/10.1038/s41586-018-0656-3.

González Fernández, R., Redondo, I., and Jorrín-Novo, J.V. (2014). Making a protein extract from plant pathogenic fungi for gel- and LC-based proteomics. Plant Proteomics: Methods and Protocols, 2nd Edition, 1072: 93-109, https://doi.org/10.1007/978-1-62703-631-3_8.

Götz, S., García-Gómez, J.M., Terol, J., Williams, T.D., Nagaraj, S.H., Nueda, M.J., Robles, M., Talón, M., Dopazo, J., and Conesa, A. (2008). High-throughput functional annotation and data mining with the Blast2GO suite. Nucleic Acids Research, 36: 3420-3435, https://doi.org/10.1093/nar/gkn176.

Granados, J.M., Avila, C., Cánovas, F.M., and Cañas, R.A. (2016). Selection and testing of reference genes for accurate RT-qPCR in adult needles and seedlings of maritime pine. Tree Genetics and Genomes 12: 60, https://doi.org/10.1007/s11295-016-1018-7.

Hawkesford, M., Horst, W., Kichey, T., Lambers, H., Schjoerring, J., Møller, I.S., and White, P. (2012). Functions of macronutrients. In Marschner's mineral nutrition of higher plants, Academic Press, 135-189, Functions of macronutrients. In Marschner's mineral nutrition of higher plants, Academic Press, 135-189, https://doi.org/10.1016/B978-0-12-384905-2.00006-6.

Hou, Y., Sun, J., Wu, B., Gao, Y., Nie, H., Nie, Z., Quan, S., Wang, Y., Cao, X., and Li, S. (2021). CPSF30-L-mediated recognition of mRNA m^6A modification controls alternative polyadenylation of nitrate signaling-related gene transcripts in *Arabidopsis*. Molecular plant, 14: 688-699, https://doi.org/10.1016/j.molp.2021.01.013.

Ikeuchi, K., and Inada, T. (2016). Ribosome-associated Asc1/RACK1 is required for endonucleolytic cleavage induced by stalled ribosome at the 3' end of nonstop mRNA. Scientific Reports, 6: 28234, https://doi.org/10.1038/srep28234.

Jamsheer, K.M., Sharma, M., Singh, D., Mannully, C.T., Jindal, S., Shukla, B.N., and Laxmi, A. (2018). FCS-like zinc finger 6 and 10 repress SnRK1 signalling in Arabidopsis. The Plant Journal, 94**:** 232-245, https://doi.org/10.1111/tpj.13854.

Jia, Z., and von Wirén, N. (2020). Signaling pathways underlying nitrogen-dependent changes in root system architecture: from model to crop species. Journal of Experimental Botany, 71: 4393–4404. https://doi.org/10.1093/jxb/eraa033

John, P., Reynolds, E.A., Prescott, A.G., and Bauchot, A.D. (1999). ACC oxidase in the biosynthesis of ethylene. In: Kanellis A.K., Chang C., Klee H., Bleecker A.B., Pech J.C., Grierson D. (eds) Biology and Biotechnology of the Plant Hormone Ethylene II. *Springer*, Dordrecht, https://doi.org/10.1007/978-94-011-4453-7_1.

Kruger, N.J., Troncoso-Ponce, M.A., and Ratcliffe, R.G. (2008). 1H NMR metabolite fingerprinting and metabolomic analysis of perchloric acid extracts from plant tissues. Nature Protocols, 3: 1001-1012, https://doi.org/10.1038/nprot.2008.64.

Li, G., Li, B., Dong, G., Feng, X., Kronzucker, and H.J., Shi, W. (2013). Ammonium-induced shoot ethylene production is associated with the inhibition of lateral root formation in *Arabidopsis*. Journal of Experimental Botany, 64:1413-1425, https://doi.org/10.1093/jxb/ert019.

Li, W., Xiang, F., Zhong, M., Zhou, L., Liu, H., Li, S., and Wang, X. (2017). Transcriptome and metabolite analysis identifies nitrogen utilization genes in tea plant (*Camellia sinensis*). Scientific Reports, 7:1-12, https://doi.org/10.1038/s41598-017-01949-0.

Li, H. (2018). Minimap2: pairwise alignment for nucleotide sequences. Bioinformatics, 34: 3094-3100, https://doi.org/10.1093/bioinformatics/bty191.

Li, F., Yi, Y., Miao, Y., Long, W., Long, T., Chen, S., Cheng, W., Zou, *et al*. (2019). N^6-methyladenosine modulates nonsense-mediated mRNA decay in human glioblastoma. Cancer Research, 79: 5785-5798, https://doi.org/10.1158/0008-5472.CAN-18-2868

Liao, Z., Chen, M., Guo, L., Gong, Y., Tang, F., Sun, X., and Tang, K. (2004). Rapid isolation of high-quality total RNA from taxus and ginkgo. Preparative Biochemistry & Biotechnology, 34: 209-214, https://doi.org/10.1081/PB-200026790.

Lima, S. A., Chipman, L. B., Nicholson, A. L., Chen, Y. H., Yee, B. A., Yeo, G. W., Coller, J., and Pasquinelli, A. E. (2017). Short poly(A) tails are a conserved feature of highly expressed genes. Nature Structural & Molecular Biology, 24: 1057-1063, https://doi.org/10.1038/nsmb.3499.

Liu, J., Wang, H., and Chua, N.H. (2015). Long noncoding RNA transcriptome of plants. Plant Biotechnology Journal, 13: 319-328, https://doi.org/10.1111/pbi.12336.

Luo, G.Z., MacQueen, A., Zheng, G., Duan, H., Dore, L.C., Lu, Z., Liu, J., Chen, K., Jia, G., Bergelson, J., and He, C. (2014). Unique features of the m6A methylome in *Arabidopsis thaliana*. Nature Communications, 5: 1-8, https://doi.org/10.1038/ncomms6630.

Madeira, F., Park, Y.M., Lee, J., Buso, N., Gur, T., Madhusoodanan, N., Basutkar, P., Tivey, A.R.N., et al. (2019). The EMBL-EBI search and sequence analysis tools APIs in 2019. Nucleic Acids Research, 47: 636-641, https://doi.org/10.1093/nar/gkz268.

Marino, D., Ariz, I., Lasa, B., Santamaría, E., Fernández-Irigoyen, J., González-Murua, C., and Aparicio-Tejo, P.M. (2016). Quantitative proteomics reveals the importance of nitrogen source to control glucosinolate metabolism in *Arabidopsis*

thaliana and *Brassica oleracea*. Journal of Experimental Botany, 67: 3313-3323, https://doi.org/10.1093/jxb/erw147.

Martínez-Pérez, M., Aparicio, F., López-Gresa, M.P., Bellés, J.M., Sánchez-Navarro, J.A., and Pallás, V. (2017). *Arabidopsis* m^6A demethylase activity modulates viral infection of a plant virus and the m^6A abundance in its genomic RNAs. Proceedings of the National Academy of Sciences, 114: 10755–10760, https://doi.org/10.1073/pnas.1703139114.

Martinez-Seidel, F., Beine-Golovchuk, O., Hsieh, Y. C., and Kopka, J. (2020). Systematic review of plant ribosome heterogeneity and specialization. Frontiers in Plant Science, 11: 948, https://doi.org/10.3389/fpls.2020.00948

Merchante, C., Brumos, J., Yun, J., Hu, Q., Spencer, K.R., Enríquez, P., Binder, B.M., Heber, S., Stepanova, A.N., and Alonso, J.M. (2015). Gene-specific translation regulation mediated by the hormone-signaling molecule EIN2. Cell, 163: 684-697, https://doi.org/10.1016/j.cell.2015.09.036.

Meyer, K.D., Saletore, Y., Zumbo, P., Elemento, O., Mason, C.E., and Jaffrey. S.R. (2012). Comprehensive analysis of mRNA methylation reveals enrichment in 3′ UTRs and near stop codons. Cell, 149: 1635-1646, https://doi.org/10.1016/j.cell.2012.05.003.

Meyer K. D. (2019). m^6A-mediated translation regulation. Biochimica et Biophysica Acta. Gene regulatory mechanisms, 1862: 301–309, https://doi.org/10.1016/j.bbagrm.2018.10.006.

Miao, Z., Zhang, T., Qi, Y., Song, J., Han, Z., and Ma, C. (2020). Evolution of the RNA N^6-methyladenosine methylome mediated by genomic duplication. Plant Physiology, 182: 345-360, https://doi.org/10.1104/pp.19.00323.

Mithran, M., Paparelli, E., Novi, G., Perata, P., and Loreti, E. (2014). Analysis of the role of the pyruvate decarboxylase gene family in *Arabidopsis thaliana* under low□oxygen conditions. Plant Biology, 16: 28-34, https://doi.org/10.1111/plb.12005.

NCBI Resource Coordinators. (2016). Database resources of the National Center for Biotechnology Information. Nucleic Acids Research, 44: 7-19, https://doi.org/10.1093/nar/gkv1290.

Ortigosa, F., Valderrama-Martín, J. M., Urbano-Gámez, J. A., García-Martín, M. L., Ávila, C., Cánovas, F. M., and Cañas, R. A. (2020). Inorganic nitrogen form determines nutrient allocation and metabolic responses in maritime pine seedlings. Plants, 9: 481, https://doi.org/10.3390/plants9040481.

Parker, M. T., Knop, K., Sherwood, A. V., Schurch, N. J., Mackinnon, K., Gould, P. D., Hall, A. J., Barton, G. J., and Simpson, G. G. (2020). Nanopore direct RNA sequencing maps the complexity of *Arabidopsis* mRNA processing and m6A modification. eLife, 9: e49658, https://doi.org/10.7554/eLife.49658

Patterson, K., Cakmak, T., Cooper, A., Lager, I., Rasmusson, A. G., and Escobar, M. A. (2010). Distinct signalling pathways and transcriptome response signatures differentiate ammonium- and nitrate-supplied plants. Plant, Cell & Environment, 33:1486–1501, https://doi.org/10.1111/j.1365-3040.2010.02158.x

Paul, S., Datta, S.K., and Datta, K. (2015). miRNA regulation of nutrient homeostasis in plants. Frontiers in Plant Science, 6, 232, https://doi.org/10.3389/fpls.2015.00232.

Prinsi, B., and Espen, L. (2018). Time-course of metabolic and proteomic responses to different nitrate/ammonium availabilities in roots and leaves of maize. International Journal of Molecular Sciences, 19: 2202, https://doi.org/10.3390/ijms19082202.

Provencher, S.W. (1993). Estimation of metabolite concentrations from localized in vivo proton NMR spectra. Magnetic Resonance in Medicine, 30: 672-679, https://doi.org/10.1002/mrm.1910300604.

Ravazzolo, L., Trevisan, S., Forestan, C., Varotto, S., Sut, S., Dall'Acqua, S., Malagoli, M., and Quaggiotti, S. (2020). Nitrate and ammonium affect the overall maize response to nitrogen availability by triggering specific and common transcriptional signatures in roots. International Journal of Molecular Sciences, 21: 686, https://doi.org/10.3390/ijms21020686.

Ritz, C., and Spiess, A.N. (2008). qpcR: an R package for sigmoidal model selection in quantitative real-time polymerase chain reaction analysis. Bioinformatics, 24: 1549-1551, https://doi.org/10.1093/bioinformatics/btn227.

Robinson, M.D., McCarthy, D.J., and Smyth, G.K. (2010). edgeR: a Bioconductor package for differential expression analysis of digital gene expression data. Bioinformatics, 26: 139-140, https://doi.org/10.1093/bioinformatics/btp616.

Romero-Rodríguez, M.C., Pascual, J., Valledor, L., and Jorrín-Novo, J.V. (2014). Improving the quality of protein identification in non-model species. Characterization of *Quercus ilex* seed and *Pinus radiata* needle proteomes by using SEQUEST and custom databases. Journal of Proteomics, 105: 85-91, https://doi.org/10.1016/j.jprot.2014.01.027.

Ruan, L., Wei, K., Wang, L., Cheng, H., Zhang, F., Wu, L., Bai, P., and Zhang, C. (2016). Characteristics of NH_4^+ and NO_3^- fluxes in tea (*Camellia sinensis*) roots measured by scanning ion-selective electrode technique. Scientific Reports, 6: 1-8, https://doi.org/10.1038/srep38370.

Sasakawa, H., and Yamamoto, Y. (1978). Comparison of the uptake of nitrate and ammonium by rice seedlings: influences of light, temperature, oxygen concentration, exogenous sucrose, and metabolic inhibitors. Plant Physiology, 62: 665-669, https://doi.org/10.1104/pp.62.4.665.

Shen, L., Liang, Z., Gu, X., Chen, Y., Teo, Z.W., Hou, X., Cai, W.M., Dedon, P.C., Liu, L., and Yu, H. (2016). N^6-Methyladenosine RNA modification regulates shoot stem cell fate in *Arabidopsis*. Developmental Cell, 38: 186–200; https://doi.org/10.1016/j.devcel.2016.06.008.

Shen, L., Liang, Z., Wong, C.E., and Yu, H. (2019). Messenger RNA modifications in plants. Trends in Plant Science, 24: 328-341, https://doi.org/10.1016/j.tplants.2019.01.005.

Stoiber, M.H., Quick, J., Egan, R., Lee, J.E., Celniker, S.E., Neely, R., Loman, N., Pennacchio, L.A., and Brown, J. (2017). De novo identification of DNA modifications enabled by genome-guided nanopore signal processing. BioRxiv, https://doi.org/10.1101/094672.

Straub T, Ludewig U, Neuhäuser B. (2017). The kinase CIPK23 inhibits ammonium transport in *Arabidopsis thaliana*. The Plant Cell, 29: 409-422, https://doi.org/10.1105/tpc.16.00806.

Sun, L., Di, D., Li, G., Kronzucker, H.J., and Shi, W. (2017). Spatio-temporal dynamics in global rice gene expression (*Oryza sativa* L.) in response to high ammonium stress. Journal of Plant Physiology, 212:94-104, https://doi.org/10.1016/j.jplph.2017.02.006.

Supek, F., Bošnjak, M., Škunca, N., and Šmuc, T. (2011). REVIGO summarizes and visualizes long lists of gene ontology terms. PloS One, 6: e21800, https://doi.org/10.1371/journal.pone.0021800.

Tian, T., Yue, L., Hengyu, Y., Qi, Y., Xin, Y., Zhou, D., Wenying, X., and Zhen, S. (2017). agriGO v2.0: a GO analysis toolkit for the agricultural community. Nucleic Acids Research 45: 122-129, https://doi.org/10.1093/nar/gkx382.

Valledor, L., and Weckwerth, W. (2014). An improved detergent-compatible gel-fractionation LC-LTQ-Orbitrap-MS workflow for plant and microbial proteomics. Methods in molecular biology (Clifton, N.J.), 1072:347–358, https://doi.org/10.1007/978-1-62703-631-3_25

Vizcaino, J.A., Cote, R.G., Csordas, A., Dianes, J.A., Fabregat, A., Foster, J.M., Griss, J., Alpi, E., *et al.* (2013). The Proteomics Identifications (PRIDE) database and associated tools: status in 2013. Nucleic Acids Research, 41: 1063-1069, https://doi.org/10.1093/nar/gks1262.

Wan, Y., Tang, K., Zhang, D., Xie, S., Zhu, X., Wang, Z., and Lang, Z. (2015). Transcriptome-wide high-throughput deep m^6A-seq reveals unique differential m^6A methylation patterns between three organs in *Arabidopsis thaliana*. Genome Biology, 16:272, https://doi.org/10.1186/s13059-015-0839-2

Wang, H., and Ng, T.B. (2000). Ginkbilobin, a novel antifungal protein from *Ginkgo biloba* seeds with sequence similarity to embryo-abundant protein. Biochemical and Biophysical Research Communications, 279: 407-411, https://doi.org/10.1006/bbrc.2000.3929.

Wang, J., Lan, P., Gao, H., Zheng, L., Li, W., and Schmidt, W. (2013). Expression changes of ribosomal proteins in phosphate- and iron-deficient *Arabidopsis* roots predict stress-specific alterations in ribosome composition. BMC Genomics, 14:783, https://doi.org/10.1186/1471-2164-14-783.

Wang, Y., Li, Y., Toth, J.I., Petroski, M.D., Zhang, Z., Zhao, J.C. (2014). N6-methyladenosine modification destabilizes developmental regulators in embryonic stem cells. Nature Cell Biology, 16:191–198, https://doi.org/10.1038/ncb2902.

Wang, W., Wang, X., Wang, X., Ahmed, S., Hussain, S., Zhang, N., Ma, Y., and Wang, S. (2019). Integration of RACK1 and ethylene signaling regulates plant growth and development in *Arabidopsis*. Plant Science, 280: 31-40, https://doi.org/10.1016/j.plantsci.2018.11.009.

Wei, L.H., Song, P., Wang, Y., Lu, Z., Tang, Q., Yu, Q., Xiao, Y., Zhang, X., Duan, H.C., and Jia, G. (2018). The m^6A reader ECT2 controls trichome morphology by affecting mRNA stability in *Arabidopsis*. The Plant Cell, 30: 968-985, https://doi.org/10.1105/tpc.17.00934.

Wu, X., Wang, J., Wu, X., Hong, Y., and Li, Q. Q. (2020). Heat shock responsive gene expression modulated by mRNA poly(A) tail length. Frontiers in Plant Science, 11: 1255, https://doi.org/10.3389/fpls.2020.01255.

Xiao, Y., Wang, Y., Tang, Q., Wei, L., Zhang, X., and Jia, G. (2018). An Elongation and Ligation-Based qPCR Amplification Method for the Radiolabeling-Free Detection of Locus Specific N6-Methyladenosine Modification. Angewandte Chemie International Edition, 57: 15995-16000, https://doi.org/10.1002/anie.201807942.

Xiong, X., Yi, C., and Peng, J. (2017). Epitranscriptomics: toward a better understanding of RNA modifications. Genomics, Proteomics & Bioinformatics, 15: 147, https://doi.org/10.1016/j.gpb.2017.03.003.

Xu, G., Fan, X., and Miller, A.J. (2012). Plant nitrogen assimilation and use efficiency. Annual Review of Plant Biology, 63: 153-182, https://doi.org/10.1146/annurev-arplant-042811-105532 .

Yang, Y., Wang, F., Wan, Q., and Ruan, J. (2018). Transcriptome analysis using RNA-Seq revealed the effects of nitrogen form on major secondary metabolite biosynthesis in tea (*Camellia sinensis*) plants. Acta Physiologiae Plantarum, 40: 127, https://doi.org/10.1007/s11738-018-2701-0.

Yang, L., Perrera, V., Saplaoura, E., Apelt, F., Bahin, M., Kramdi, A., Olas, J., Mueller-Roeber, B., *et al.* (2019). m^5C methylation guides systemic transport of messenger RNA over graft junctions in plants. Current Biology, 29: 2465-2476, https://doi.org/10.1016/j.cub.2019.06.042.

Zhong, S., Li, H., Bodi, Z., Button, J., Vespa, L., Herzog, M., and Fray, R.G. (2008). MTA is an *Arabidopsis* messenger RNA adenosine methylase and interacts with a homolog of a sex-specific splicing factor. The Plant Cell, 20:1278–1288, https://doi.org/10.1105/tpc.108.058883.

Zhou, L., Tian, S., and Qin, G. (2019). RNA methylomes reveal the m^6A-mediated regulation of DNA demethylase gene SlDML2 in tomato fruit ripening. Genome Biology, 20: 156, https://doi.org/10.1186/s13059-019-1771-7.

FIGURE LEGENDS

Figure 1. Main trend of metabolites in the roots of control and NH_4^+-treated seedlings at 24 hours post-irrigation. Blue columns correspond to control plants; red columns correspond to 3 mM NH_4^+ supply. Differences between treatments were determined with a t-test. Significant differences are indicated with asterisks on top of the columns: * at $P < 0.05$. Error bars show SE with $n = 3$. PEP: phosphoenolpyruvate.

Figure 2. Main DRS transcriptomics results. **A.** Size distribution of reads obtained through DRS-ONT sequencing. **B.** MA plot containing all detected transcripts. Blue points correspond to significantly downregulated transcripts in maritime pine roots at 24 h after the treatment with 3 mM ammonium. Red points correspond to significantly upregulated transcripts in maritime pine roots at 24 h after the treatment with 3 mM ammonium. **C.** Significant GO terms from significant DE transcripts after a SEA analysis. **D.** Comparison between DRS and RT-qPCR results from different transcripts with significant differential expression in the DRS analysis.

Figure 3. Epitranscriptomics modification results from Tombo software analysis. **A.** Volcano plot of the detected epitranscriptomics modifications. Yellow points correspond to modifications with *P*-values lower than 0.05 but with an absolute logFC value lower than 0.5. Blue points correspond to modifications with an absolute logFC value higher than 0.5 but with *P*-values higher than 0.05. Red points correspond to significant DE modifications with an absolute logFC value higher than 0.5 and *P*-values lower than 0.05. **B.** Percentage of detected modifications per nucleobase. Yellow columns correspond to control samples. Purple columns correspond to 3 mM ammonium treated samples. **C.** Scatter plot and correlation between detected modifications using Tombo software and transcript amounts determined by DRS sequencing. **D.** Significant GO terms from significant DE modifications after a SEA analysis. **E.** Comparison between DRS and SELECT results from different transcript modified positions with significant differential modification in the Tombo analysis.

Figure 4. m^6A identification results using the bioinformatics pipeline Nanom6A. **A.** Distribution of the identified m^6A all along the transcripts. **B.** Distribution of the identified m^6A along each part of the transcripts: 5'UTR, CDS and 3'UTR respectively. **C.** Percentage of identified m^6A for each different variant (kmer) of the consensus sequence RRACH for adenine methylation. **D.** Scatter plot and correlations between m^6A modification ratio and transcript amount from DRS sequencing. **E.** Poly(A) length of the transcripts identified in the DRS sequencing. **F.** Scatter plot and correlations between poly(A) length and m^6A modification ratio. **G.** Scatter plot and correlations between poly(A) length and transcript amount from DRS sequencing.

Figure 5. Differential expression proteomics results. **A.** Volcano plot of the identified proteins. Yellow points correspond to modifications with *P*-values lower than 0.05 but with an absolute logFC value lower than 0.5. Red points correspond to significant DE modifications with an absolute logFC value higher than 0.5 and *P*-values lower than 0.05. **B.** Significant GO terms from significant DE proteins after a SEA analysis. **C.** Scatter plot and correlations between m^6A modification ratios and protein amounts. **D.** Scatter plot and correlations between transcript amounts from DRS sequencing and protein amounts.

Figure 6. Common results among different omics approaches. **A.** Genes with significant expressions in more than one omics approach. Red boxes correspond to upregulated transcripts and proteins. Blue boxes correspond to downregulated transcripts and proteins. Yellow boxes correspond to significant differentially modified positions in the transcripts. **B.** Venn diagram of significant GO terms in the different omics approaches. **C.** Heatmap of significant GO terms shared by at least two omics approaches. **D.** Heatmap of genes that produce proteins involved in ribosome and translation. Ribosomal protein equivalences obtained from Martinez-Seidel et al. (2020). Red boxes correspond to upregulated transcripts and proteins. Blue boxes correspond to downregulated transcripts and proteins. Yellow boxes correspond to significant differentially modified positions in the transcripts.

Figure 7. Schematic representation of functional results obtained through the omics integrative approach. NH_4^+ triggers carbon and nitrogen metabolism, ethylene biosynthesis and signaling and translation responses. Geometric red and blue forms indicate upregulation and downregulation respectively of transcripts, RNA nucleoside modifications, proteins, and metabolites.

Supplemental Information

Supplemental Table 1. Direct RNA sequencing information for each sample run.

Supplemental Table 2. Primer list.

Supplemental Methods 1. Extended Materials and Methods.

Supplemental Figure 1. Heatmap of root metabolites. The analysis was done with Metaboanalyst using the Euclidean distance and Ward clustering algorithm. Class 0 (blue group) corresponds with control samples irrigated with distilled water. Class 3 (red group) corresponds with seedlings irrigated with 3 mM NH_4^+.

Supplemental Figure 2. Significant GO terms after SEA analysis using the DRS results.

Supplemental Figure 3. Scatter plot and correlations between the transcript amounts and the modification ratios detected using Tombo software for each nucleoside.

Supplemental Figure 4. Significant GO terms after SEA analysis using the epitranscriptomics results obtained from Tombo software.

Supplemental Figure 5. Scatter plot and correlations between the poly(A) length and the modification ratios detected using Tombo software for each nucleoside and global results.

Supplemental Figure 6. Significant GO terms after SEA analysis using the proteomics results.

Supplemental Figure 7. Scatter plot and correlations between the protein amounts and the modification ratios detected using Tombo software for each nucleoside and global results.

Supplemental Figure 8. Glutamine synthetase activity in maritime pine roots under ammonium nutrition. The results are the mean of three independent experiments using biological pools. Error bars correspond to SE. Enzymatic determinations were described in Supplemental Methods 1.

Supplemental Dataset 1. Normalized data from root metabolite profiling.

Supplemental Dataset 2. Whole root DRS differential expression results. DE transcripts upregulated are in highlighted red. DE transcripts downregulated are in highlighted blue.

Supplemental Dataset 3. SEA whole root DRS differential overexpressed transcripts results.

Supplemental Dataset 4. DRS differential modification results in pine roots under ammonium nutrition. DE transcripts overmodified are in highlighted red. DE transcripts undermodified are in highlighted blue.

Supplemental Dataset 5. Transcripts with upregulated and downregulated modifications at the same time.

Supplemental Dataset 6. SEA of transcripts with significant epitranscriptomic modifications in pine roots under ammonium nutrition.

Supplemental Dataset 7. Identified differential m^6A positions coincident with DRS differential modification detected by Tombo software in the three close positions context. DE transcripts overmodified are in highlighted red. DE transcripts undermodified are in highlighted blue.

Supplemental Dataset 8. Whole root differential proteomics results. DE proteins upregulated are in highlighted red. DE proteins downregulated are in highlighted blue.

Supplemental Dataset 9. SEA results of proteins overexpressed in pine roots under ammonium nutrition.

Supplemental Dataset 10. Elements with significant changes at least in two experimental approaches.

Supplemental Dataset 11. Commons significant GO terms between omics analyses.

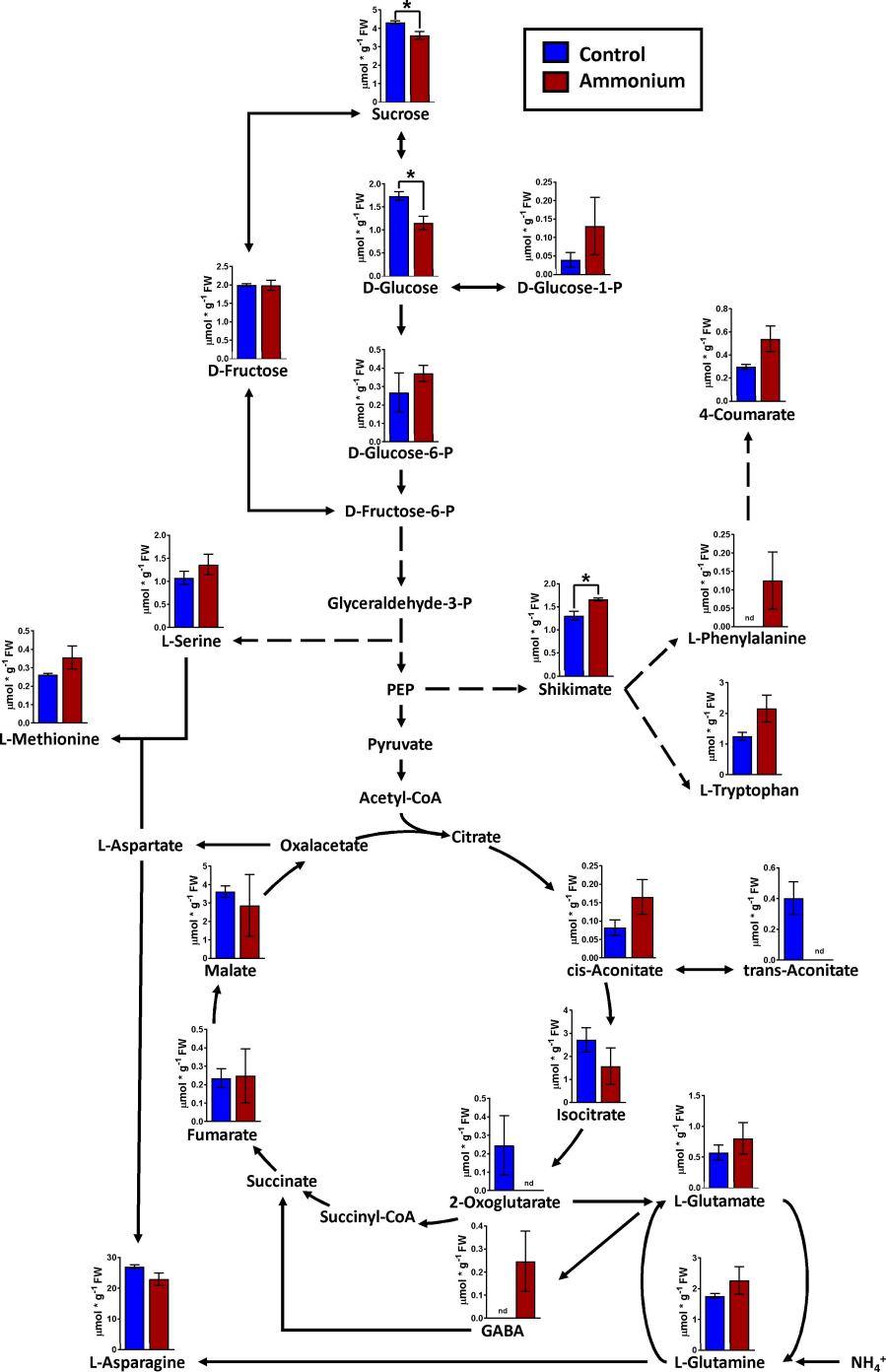
Control
Ammonium
Sucrose
D-Glucose
D-Glucose-1-P
D-Fructose
D-Glucose-6-P
D-Fructose-6-P
4-Coumarate
Glyceraldehyde-3-P
L-Serine
L-Phenylalanine
L-Methionine
PEP
Shikimate
L-Tryptophan
Pyruvate
Acetyl-CoA
L-Aspartate
Oxalacetate
Citrate
Malate
cis-Aconitate
trans-Aconitate
Isocitrate
Fumarate
2-Oxoglutarate
L-Glutamate
Succinate
Succinyl-CoA
GABA
L-Asparagine
L-Glutamine
NH4+
µmol * g-1 FW
nd

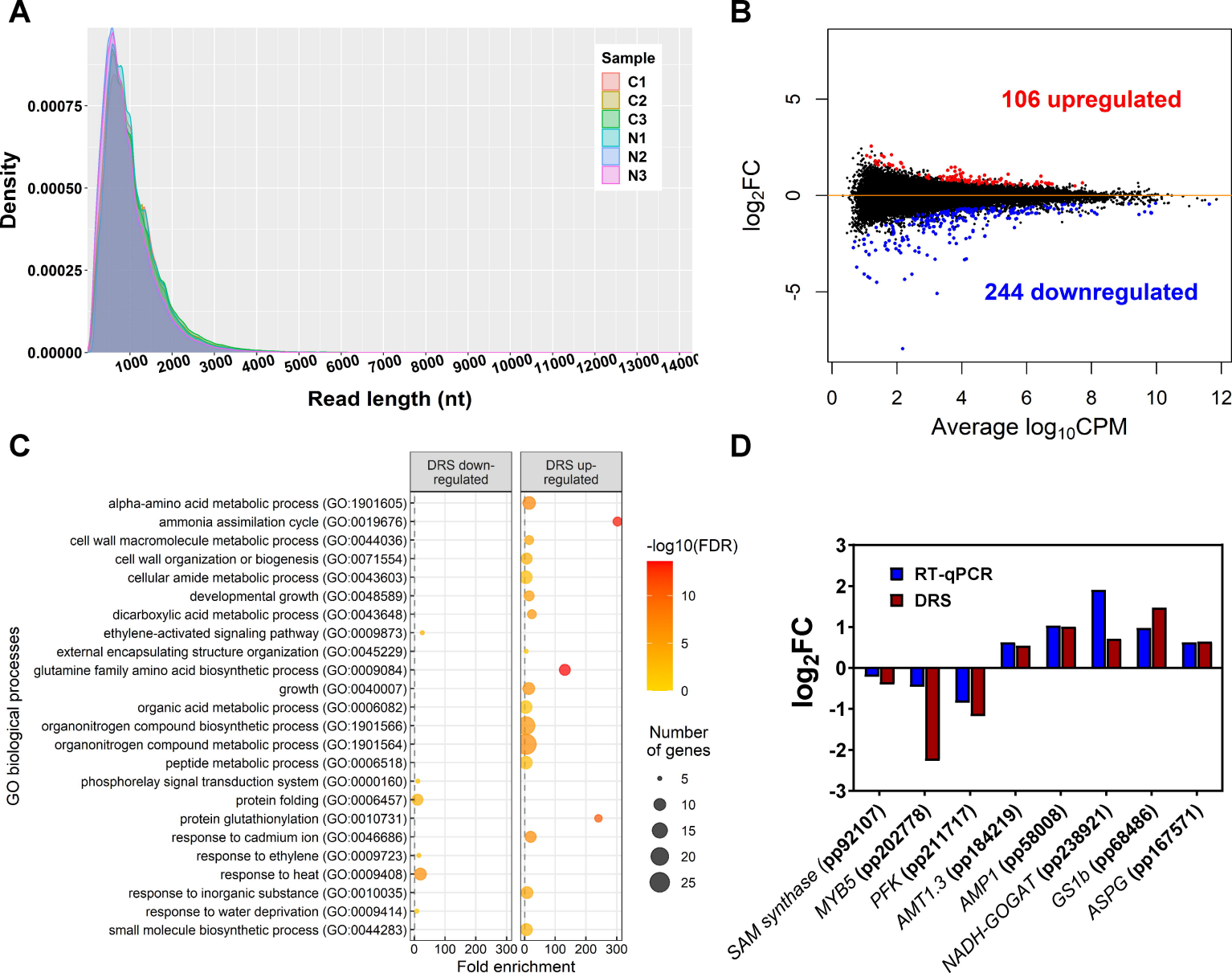
A
Sample
C1
C2
C3
N1
N2
N3
Density
0.00075
0.00050
0.00025
0.00000
1000 2000 3000 4000 5000 6000 7000 8000 9000 10000 11000 12000 13000 14000
Read length (nt)
B
106 upregulated
244 downregulated
log2FC
5
0
-5
0 2 4 6 8 10 12
Average log10CPM
C
DRS down-regulated
DRS up-regulated
GO biological processes
alpha-amino acid metabolic process (GO:1901605)
ammonia assimilation cycle (GO:0019676)
cell wall macromolecule metabolic process (GO:0044036)
cell wall organization or biogenesis (GO:0071554)
cellular amide metabolic process (GO:0043603)
developmental growth (GO:0048589)
dicarboxylic acid metabolic process (GO:0043648)
ethylene-activated signaling pathway (GO:0009873)
external encapsulating structure organization (GO:0045229)
glutamine family amino acid biosynthetic process (GO:0009084)
growth (GO:0040007)
organic acid metabolic process (GO:0006082)
organonitrogen compound biosynthetic process (GO:1901566)
organonitrogen compound metabolic process (GO:1901564)
peptide metabolic process (GO:0006518)
phosphorelay signal transduction system (GO:0000160)
protein folding (GO:0006457)
protein glutathionylation (GO:0010731)
response to cadmium ion (GO:0046686)
response to ethylene (GO:0009723)
response to heat (GO:0009408)
response to inorganic substance (GO:0010035)
response to water deprivation (GO:0009414)
small molecule biosynthetic process (GO:0044283)
0 100 200 300
Fold enrichment
-log10(FDR)
10
5
0
Number of genes
5
10
15
20
25
D
RT-qPCR
DRS
log2FC
3
2
1
0
-1
-2
-3
SAM synthase (pp92107)
MYB5 (pp202778)
PFK (pp211717)
AMT1.3 (pp184219)
AMP1 (pp58008)
NADH-GOGAT (pp238921)
GS1b (pp68486)
ASPG (pp167571)

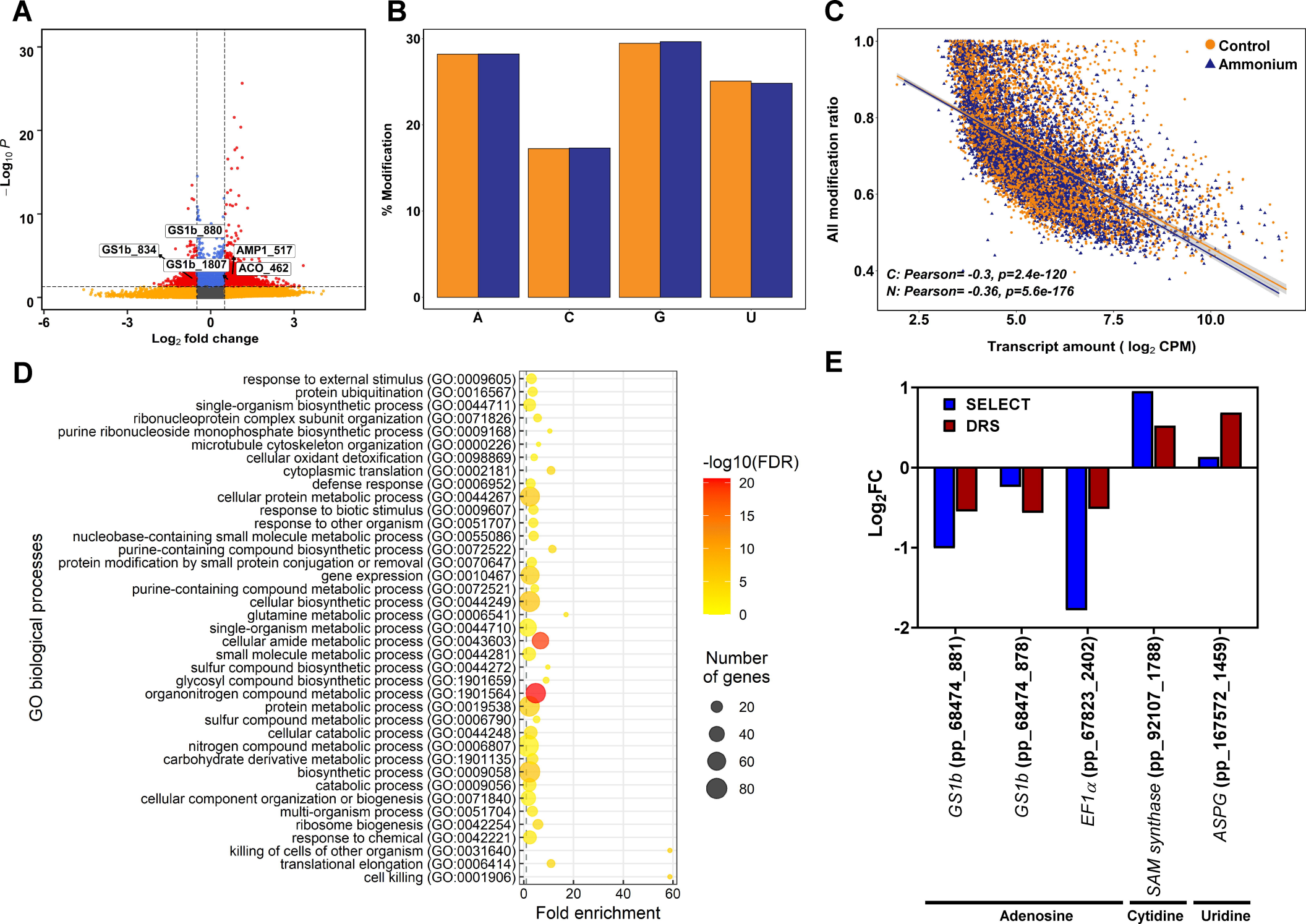
A
−Log10 P
Log2 fold change
GS1b_880
GS1b_834
GS1b_1807
AMP1_517
ACO_462
B
% Modification
A
C
G
U
C
All modification ratio
Transcript amount (log2 CPM)
Control
Ammonium
C: Pearson= -0.3, p=2.4e-120
N: Pearson= -0.36, p=5.6e-176
D
GO biological processes
response to external stimulus (GO:0009605)
protein ubiquitination (GO:0016567)
single-organism biosynthetic process (GO:0044711)
ribonucleoprotein complex subunit organization (GO:0071826)
purine ribonucleoside monophosphate biosynthetic process (GO:0009168)
microtubule cytoskeleton organization (GO:0000226)
cellular oxidant detoxification (GO:0098869)
cytoplasmic translation (GO:0002181)
defense response (GO:0006952)
cellular protein metabolic process (GO:0044267)
response to biotic stimulus (GO:0009607)
response to other organism (GO:0051707)
nucleobase-containing small molecule metabolic process (GO:0055086)
purine-containing compound biosynthetic process (GO:0072522)
protein modification by small protein conjugation or removal (GO:0070647)
gene expression (GO:0010467)
purine-containing compound metabolic process (GO:0072521)
cellular biosynthetic process (GO:0044249)
glutamine metabolic process (GO:0006541)
single-organism metabolic process (GO:0044710)
cellular amide metabolic process (GO:0043603)
small molecule metabolic process (GO:0044281)
sulfur compound biosynthetic process (GO:0044272)
glycosyl compound biosynthetic process (GO:1901659)
organonitrogen compound metabolic process (GO:1901564)
protein metabolic process (GO:0019538)
sulfur compound metabolic process (GO:0006790)
cellular catabolic process (GO:0044248)
nitrogen compound metabolic process (GO:0006807)
carbohydrate derivative metabolic process (GO:1901135)
biosynthetic process (GO:0009058)
catabolic process (GO:0009056)
cellular component organization or biogenesis (GO:0071840)
multi-organism process (GO:0051704)
ribosome biogenesis (GO:0042254)
response to chemical (GO:0042221)
killing of cells of other organism (GO:0031640)
translational elongation (GO:0006414)
cell killing (GO:0001906)
Fold enrichment
-log10(FDR)
Number of genes
E
Log2FC
SELECT
DRS
GS1b (pp_68474_881)
GS1b (pp_68474_878)
EF1α (pp_67823_2402)
SAM synthase (pp_92107_1788)
ASPG (pp_167572_1459)
Adenosine
Cytidine
Uridine

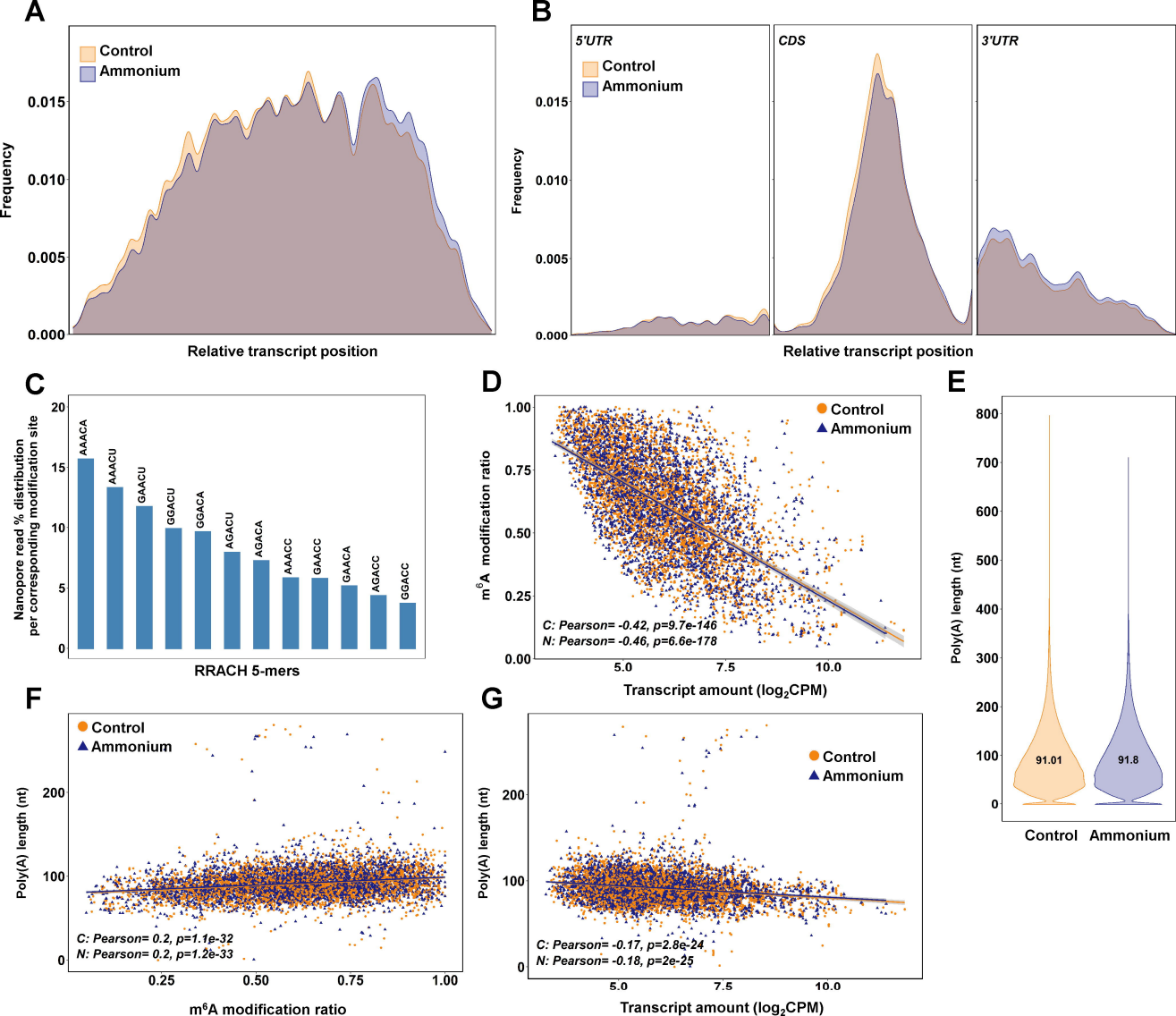
A
Control
Ammonium
Frequency
0.015
0.010
0.005
0.000
Relative transcript position
B
5'UTR
CDS
3'UTR
Control
Ammonium
Frequency
0.015
0.010
0.005
0.000
Relative transcript position
C
Nanopore read % distribution per corresponding modification site
AAACA
AAACU
GAACU
GGACU
GGACA
AGACU
AGACA
AAACC
GAACC
GAACA
AGACC
GGACC
RRACH 5-mers
D
Control
Ammonium
m6A modification ratio
C: Pearson= -0.42, p=9.7e-146
N: Pearson= -0.46, p=6.6e-178
Transcript amount (log2CPM)
E
Poly(A) length (nt)
91.01
91.8
Control
Ammonium
F
Control
Ammonium
Poly(A) length (nt)
C: Pearson= 0.2, p=1.1e-32
N: Pearson= 0.2, p=1.2e-33
m6A modification ratio
G
Control
Ammonium
Poly(A) length (nt)
C: Pearson= -0.17, p=2.8e-24
N: Pearson= -0.18, p=2e-25
Transcript amount (log2CPM)

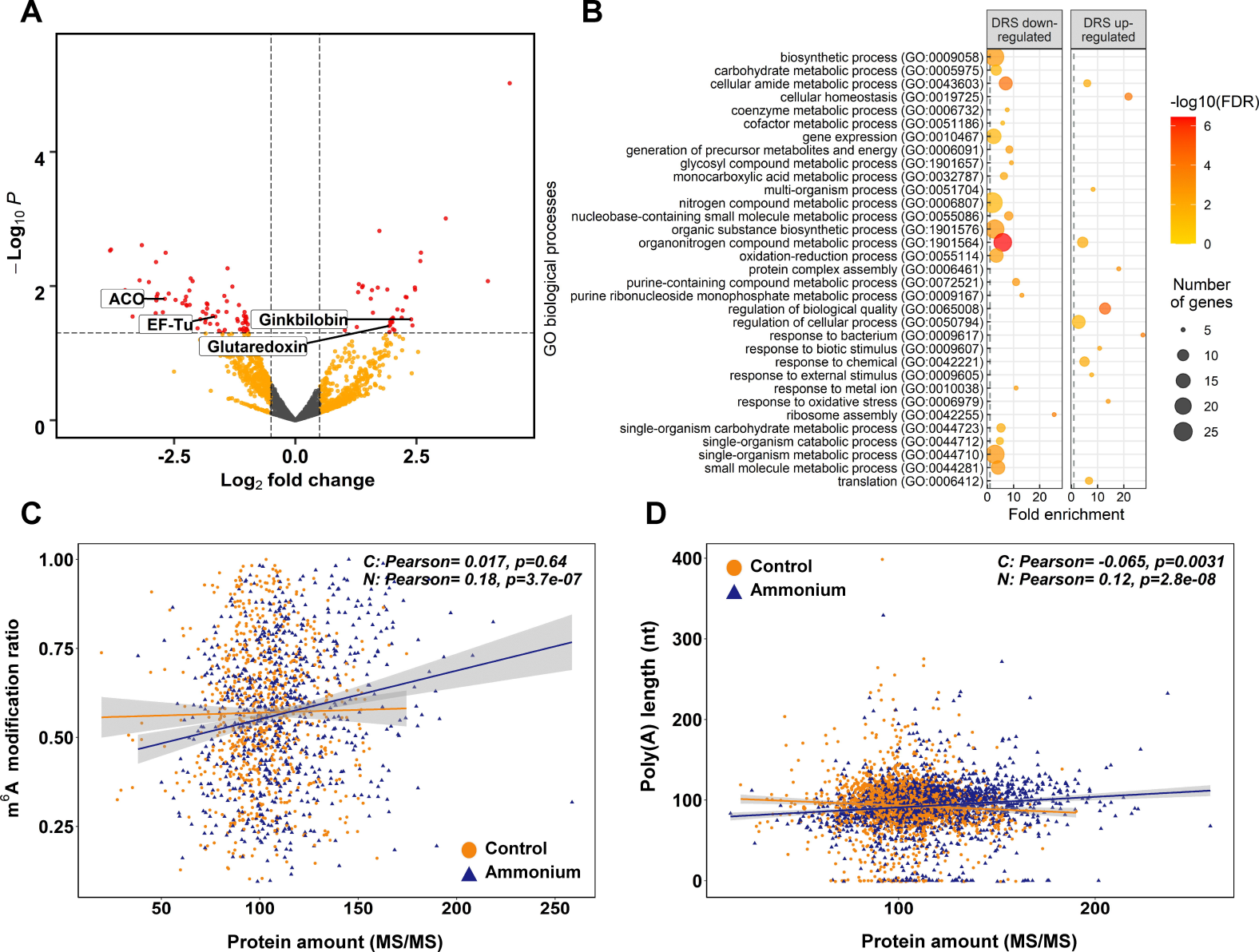
A
−Log10 P
Log2 fold change
ACO
EF-Tu
Ginkbilobin
Glutaredoxin
B
DRS down-regulated
DRS up-regulated
GO biological processes
biosynthetic process (GO:0009058)
carbohydrate metabolic process (GO:0005975)
cellular amide metabolic process (GO:0043603)
cellular homeostasis (GO:0019725)
coenzyme metabolic process (GO:0006732)
cofactor metabolic process (GO:0051186)
gene expression (GO:0010467)
generation of precursor metabolites and energy (GO:0006091)
glycosyl compound metabolic process (GO:1901657)
monocarboxylic acid metabolic process (GO:0032787)
multi-organism process (GO:0051704)
nitrogen compound metabolic process (GO:0006807)
nucleobase-containing small molecule metabolic process (GO:0055086)
organic substance biosynthetic process (GO:1901576)
organonitrogen compound metabolic process (GO:1901564)
oxidation-reduction process (GO:0055114)
protein complex assembly (GO:0006461)
purine-containing compound metabolic process (GO:0072521)
purine ribonucleoside monophosphate metabolic process (GO:0009167)
regulation of biological quality (GO:0065008)
regulation of cellular process (GO:0050794)
response to bacterium (GO:0009617)
response to biotic stimulus (GO:0009607)
response to chemical (GO:0042221)
response to external stimulus (GO:0009605)
response to metal ion (GO:0010038)
response to oxidative stress (GO:0006979)
ribosome assembly (GO:0042255)
single-organism carbohydrate metabolic process (GO:0044723)
single-organism catabolic process (GO:0044712)
single-organism metabolic process (GO:0044710)
small molecule metabolic process (GO:0044281)
translation (GO:0006412)
Fold enrichment
-log10(FDR)
Number of genes
C
C: Pearson= 0.017, p=0.64
N: Pearson= 0.18, p=3.7e-07
m6A modification ratio
Protein amount (MS/MS)
Control
Ammonium
D
C: Pearson= -0.065, p=0.0031
N: Pearson= 0.12, p=2.8e-08
Poly(A) length (nt)
Protein amount (MS/MS)
Control
Ammonium

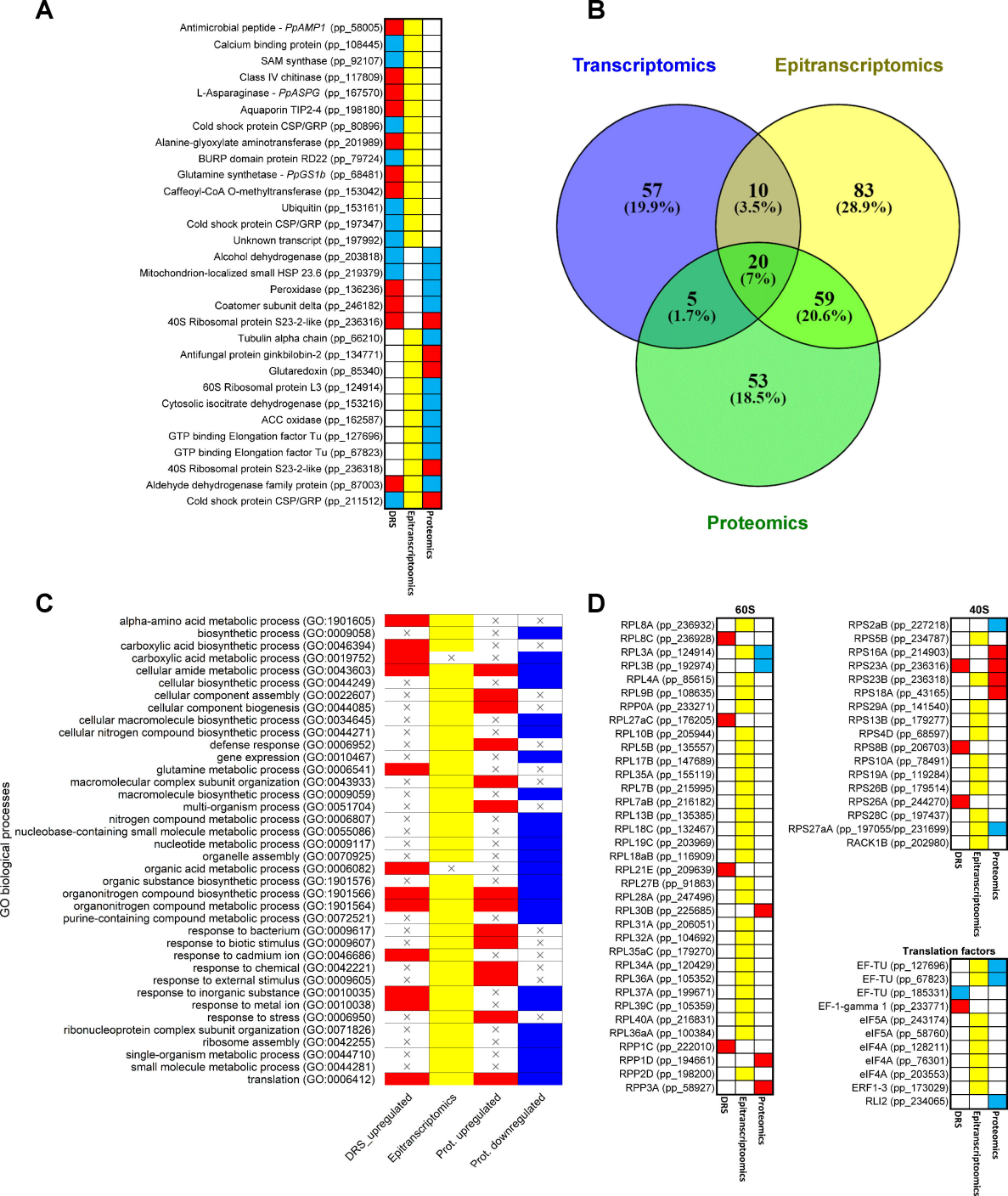
A
Antimicrobial peptide - PpAMP1 (pp_58005)
Calcium binding protein (pp_108445)
SAM synthase (pp_92107)
Class IV chitinase (pp_117809)
L-Asparaginase - PpASPG (pp_167570)
Aquaporin TIP2-4 (pp_198180)
Cold shock protein CSP/GRP (pp_80896)
Alanine-glyoxylate aminotransferase (pp_201989)
BURP domain protein RD22 (pp_79724)
Glutamine synthetase - PpGS1b (pp_68481)
Caffeoyl-CoA O-methyltransferase (pp_153042)
Ubiquitin (pp_153161)
Cold shock protein CSP/GRP (pp_197347)
Unknown transcript (pp_197992)
Alcohol dehydrogenase (pp_203818)
Mitochondrion-localized small HSP 23.6 (pp_219379)
Peroxidase (pp_136236)
Coatomer subunit delta (pp_246182)
40S Ribosomal protein S23-2-like (pp_236316)
Tubulin alpha chain (pp_66210)
Antifungal protein ginkbilobin-2 (pp_134771)
Glutaredoxin (pp_85340)
60S Ribosomal protein L3 (pp_124914)
Cytosolic isocitrate dehydrogenase (pp_153216)
ACC oxidase (pp_162587)
GTP binding Elongation factor Tu (pp_127696)
GTP binding Elongation factor Tu (pp_67823)
40S Ribosomal protein S23-2-like (pp_236318)
Aldehyde dehydrogenase family protein (pp_87003)
Cold shock protein CSP/GRP (pp_211512)
DRS
Epitranscriptoomics
Proteomics
B
Transcriptomics
Epitranscriptomics
Proteomics
57 (19.9%)
10 (3.5%)
83 (28.9%)
20 (7%)
5 (1.7%)
59 (20.6%)
53 (18.5%)
C
GO biological processes
alpha-amino acid metabolic process (GO:1901605)
biosynthetic process (GO:0009058)
carboxylic acid biosynthetic process (GO:0046394)
carboxylic acid metabolic process (GO:0019752)
cellular amide metabolic process (GO:0043603)
cellular biosynthetic process (GO:0044249)
cellular component assembly (GO:0022607)
cellular component biogenesis (GO:0044085)
cellular macromolecule biosynthetic process (GO:0034645)
cellular nitrogen compound biosynthetic process (GO:0044271)
defense response (GO:0006952)
gene expression (GO:0010467)
glutamine metabolic process (GO:0006541)
macromolecular complex subunit organization (GO:0043933)
macromolecule biosynthetic process (GO:0009059)
multi-organism process (GO:0051704)
nitrogen compound metabolic process (GO:0006807)
nucleobase-containing small molecule metabolic process (GO:0055086)
nucleotide metabolic process (GO:0009117)
organelle assembly (GO:0070925)
organic acid metabolic process (GO:0006082)
organic substance biosynthetic process (GO:1901576)
organonitrogen compound biosynthetic process (GO:1901566)
organonitrogen compound metabolic process (GO:1901564)
purine-containing compound metabolic process (GO:0072521)
response to bacterium (GO:0009617)
response to biotic stimulus (GO:0009607)
response to cadmium ion (GO:0046686)
response to chemical (GO:0042221)
response to external stimulus (GO:0009605)
response to inorganic substance (GO:0010035)
response to metal ion (GO:0010038)
response to stress (GO:0006950)
ribonucleoprotein complex subunit organization (GO:0071826)
ribosome assembly (GO:0042255)
single-organism metabolic process (GO:0044710)
small molecule metabolic process (GO:0044281)
translation (GO:0006412)
DRS_upregulated
Epitranscriptomics
Prot. upregulated
Prot. downregulated
D
60S
RPL8A (pp_236932)
RPL8C (pp_236928)
RPL3A (pp_124914)
RPL3B (pp_192974)
RPL4A (pp_85615)
RPL9B (pp_108635)
RPP0A (pp_233271)
RPL27aC (pp_176205)
RPL10B (pp_205944)
RPL5B (pp_135557)
RPL17B (pp_147689)
RPL35A (pp_155119)
RPL7B (pp_215995)
RPL7aB (pp_216182)
RPL13B (pp_135385)
RPL18C (pp_132467)
RPL19C (pp_203969)
RPL18aB (pp_116909)
RPL21E (pp_209639)
RPL27B (pp_91863)
RPL28A (pp_247496)
RPL30B (pp_225685)
RPL31A (pp_206051)
RPL32A (pp_104692)
RPL35aC (pp_179270)
RPL34A (pp_120429)
RPL36A (pp_105352)
RPL37A (pp_199671)
RPL39C (pp_105359)
RPL40A (pp_216831)
RPL36aA (pp_100384)
RPP1C (pp_222010)
RPP1D (pp_194661)
RPP2D (pp_198200)
RPP3A (pp_58927)
DRS
Epitranscriptoomics
Proteomics
40S
RPS2aB (pp_227218)
RPS5B (pp_234787)
RPS16A (pp_214903)
RPS23A (pp_236316)
RPS23B (pp_236318)
RPS18A (pp_43165)
RPS29A (pp_141540)
RPS13B (pp_179277)
RPS4D (pp_68597)
RPS8B (pp_206703)
RPS10A (pp_78491)
RPS19A (pp_119284)
RPS26B (pp_179514)
RPS26A (pp_244270)
RPS28C (pp_197437)
RPS27aA (pp_197055/pp_231699)
RACK1B (pp_202980)
DRS
Epitranscriptoomics
Proteomics
Translation factors
EF-TU (pp_127696)
EF-TU (pp_67823)
EF-TU (pp_185331)
EF-1-gamma 1 (pp_233771)
eIF5A (pp_243174)
eIF5A (pp_58760)
eIF4A (pp_128211)
eIF4A (pp_76301)
eIF4A (pp_203553)
ERF1-3 (pp_173029)
RLI2 (pp_234065)
DRS
Epitranscriptoomics
Proteomics

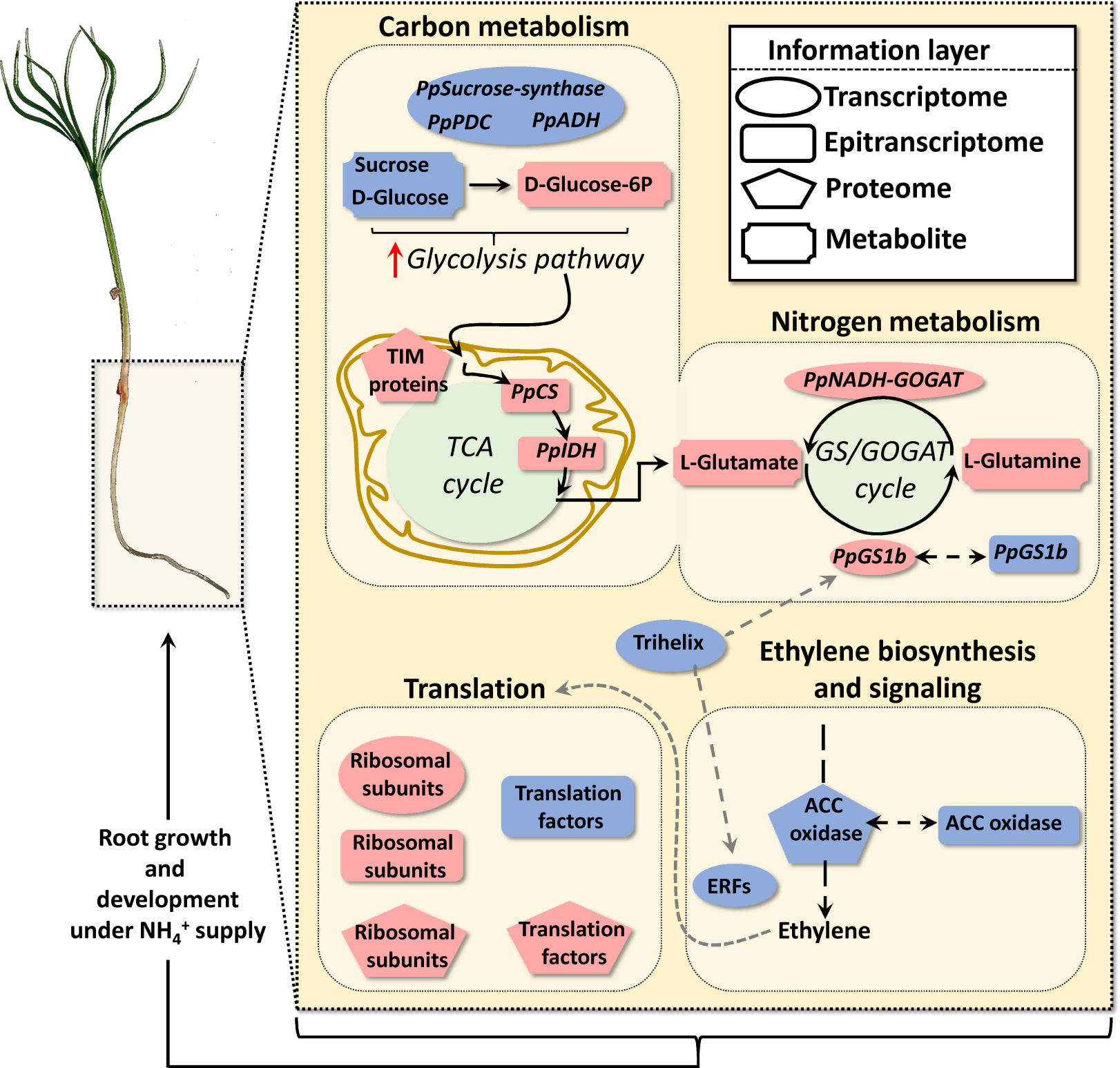
Carbon metabolism
Information layer
Transcriptome
Epitranscriptome
Proteome
Metabolite
PpSucrose-synthase
PpPDC
PpADH
Sucrose
D-Glucose
D-Glucose-6P
Glycolysis pathway
TIM proteins
PpCS
PpIDH
TCA cycle
Nitrogen metabolism
PpNADH-GOGAT
L-Glutamate
GS/GOGAT cycle
L-Glutamine
PpGS1b
PpGS1b
Trihelix
Ethylene biosynthesis and signaling
Translation
Ribosomal subunits
Translation factors
Ribosomal subunits
Ribosomal subunits
Translation factors
ACC oxidase
ACC oxidase
ERFs
Ethylene
Root growth and development under NH4+ supply